

REPORT DOCUMENTATION PAGE

Form Approved
OMB No. 0704-0188

Public reporting burden for this collection of information is estimated to average 1 hour per response, including the time for reviewing instructions, searching existing data sources, gathering and maintaining the data needed, and completing and reviewing the collection of information. Send comments regarding this burden estimate or any other aspect of this collection of information, including suggestions for reducing this burden, to Washington Headquarters Services, Directorate for Information Operations and Reports, 1215 Jefferson Davis Highway, Suite 1204, Arlington, VA 22202-4302, and to the Office of Management and Budget, Paperwork Reduction Project (0704-0188), Washington, DC 20503.

1. AGENCY USE ONLY (Leave blank)	2. REPORT DATE 15 August 1995	3. REPORT TYPE AND DATES COVERED Final 1-Sept-1994 15-Aug-1995
4. TITLE AND SUBTITLE Chemical Vapor Infiltration Design Optimization		5. FUNDING NUMBERS F49620-94-C-0070
6. AUTHOR(S) Dennis Torok & Stefano Mereu Dan Boss & Sankar Sambasivan		

7. PERFORMING ORGANIZATION NAME(S) AND ADDRESS(ES) Fluid Dynamics International 500 Davis Street, Suite 600 Evanston, IL 60201	Northwestern University 633 Clark Street Evanston, IL 60208	8. PERFORMING ORGANIZATION AFOSR-TR-95 06061
---	---	--

9. SPONSORING/MONITORING AGENCY NAME(S) AND ADDRESS(ES) USAF, XXXX Air Force Office of Scientific Research 110 Duncan Ave. Suite B115 Bolling AFB, DC 20332-0001	NA	AGENCY REPORT NUMBER F49620- 94-C-0070
---	----	--

11. SUPPLEMENTARY NOTES	DTIC SELECTED OCT 20 1995 G
12a. DISTRIBUTION/AVAILABILITY STATEMENT Approved for public release, Distribution unlimited	

13. ABSTRACT (Maximum 200 words) The construction, execution, and experimental validation of a computer model for isothermal CVI processes. The feasibility of incorporating the model into a commercial CFD code, FIDAP, is investigated. Model validations were made using methyl trichlorosilane and hydrogen. Comparisons revealed encouraging agreement between the model predictions and experimental data. The model predicted the correct trends of the densification rate as a function of temperature and pressure while slightly overestimating the densification rate as a function of time.

19951018 012

DTIC QUALITY INSPECTED 3

14. SUBJECT TERMS CVI, Numerical Simulation, Materials Processing, FIDAP			15. NUMBER OF PAGES 60
			16. PRICE CODE
17. SECURITY CLASSIFICATION OF REPORT	18. SECURITY CLASSIFICATION OF THIS PAGE	19. SECURITY CLASSIFICATION OF ABSTRACT	20. LIMITATION OF ABSTRACT

NSN 7540-01-280-5500

Standard Form 298 (Rev 2-89)
Prescribed by ANSI Std Z39-18
298-102

REF D

CHEMICAL VAPOR INFILTRATION

DESIGN OPTIMIZATION

U.S. Department of Defense

Small Business Technology Transfer Grant (STTR)

Accession For	
NTIS	CRA&I <input checked="" type="checkbox"/>
DTIC	TAB <input type="checkbox"/>
Unannounced <input type="checkbox"/>	
Justification	
By _____	
Distribution /	
Availability Codes	
Dist	Avail and/or Special
A-1	

Dennis Torok, Ph.D.

Stefano Mereu, Ph.D.

Fluid Dynamics International

Mr. Daniel Boss

Sankar Sambasivan, Ph.D.

BIRL

FLUID DYNAMICS INTERNATIONAL NORTHWESTERN UNIVERSITY

500 DAVIS STREET SUITE 600

633 CLARK STREET

EVANSTON, IL 60201

EVANSTON, IL 60208-1110

TECHNICAL SUMMARY

The objective of the study was to construct, execute, and experimentally validate a computer model for isothermal CVI processes. The feasibility of incorporating the model into a commercial computational fluid dynamics analysis code, FIDAP, was investigated. Enhancements, if necessary, were documented for further developmental efforts. Model validations were made for a CVI process using methyl trichlorosilane and hydrogen. The modeling effort focused on:

1. evaluation of the feasibility of incorporating a densification model for the infiltration of chemical vapors within a cloth preform into FIDAP, a general purpose commercial finite element CFD code.
2. validation of the model via comparison with experimental infiltration results from actual preforms.

The comparisons revealed encouraging agreement between the model prediction and the experimental data with the model predicting the correct trends of the densification rate as a function of temperature and pressure, while slightly overestimating the densification rate as a function of time.

The results appear quite promising in view of the fact that the input parameters have been largely obtained from the literature, with no empirical relationship except the ones regarding the structure of the preform. The results indicate that better reaction data and better representation of preform architecture are necessary before more quantitative agreement between experimental data and numerical predictions can be attained.

FDI has shown, through comparison with experimental CVI results performed by BIRL, that modifications to an existing commercial fluid dynamics software code, FIDAP, can provide industrial users with a tool to aid in the design and optimization of reactors and CVI processes. Continuation of this work in a Phase II study would provide, from a users point of view, access to continuously updated, state of the art models for chemical vapor infiltration.

INTRODUCTION

Chemical vapor infiltration (CVI) has held the promise for significant advances in materials performance for over 15 years. The key advantages of these advanced composites are their higher specific mechanical properties, increased service temperature, and resistance to creep. The Air Force derives a particular benefit from the higher specific properties and increased service temperature because of the need to increase thrust-to-weight ratio for improved aircraft performance and fuel economy. An enabling technology for these advanced composites is chemical vapor deposition/infiltration which is used to densify the CMC and C/C structures, apply interfacial coatings to fibrous preforms, and deposit protective coatings.

A number of variations on CVI, including isothermal, forced-flow, thermal-gradient, forced-flow thermal-gradient, pulsed, and microwave-heated, have been developed in this time, but only the isothermal method is used commercially. (For the balance of our discussion, CVI will denote the isothermal process unless otherwise noted.) However, it has been limited by problems with process variability and repeatability, high-development costs, part thickness limitations, and difficulties in scale-up processes in the production environment. Process control for CVI has advanced to using electronic controllers for precursor flow, pressure, and temperature. However, which of the parameters are truly important to the process are not known so the control philosophy has degraded to a "control everything" approach. Problems of repeatability, cost, and scale-up persist despite improvements in process controllers which indicates that there are significant gaps in the basic understanding of the effects of deposition parameter variations on the process. These gaps in understanding are particularly apparent when developing processing conditions for new coatings, trying to optimize processing conditions, and when scale-up to larger reactors is required.

Current CVI manufacturing processes for composites face several limitations, such as cost, repeatability, and scale-up, which could all be addressed through the validation of a computational fluid-dynamic model for the process. A valid model would allow optimization of current manufacturing processes for C/C and CMC which would result in lower costs, increased repeatability, and optimized equipment designs. The lack of a predictive model for these manufacturing processes forces a multi-step densification process which requires several intermediate inspections of the parts to determine the amount of additional processing time required to achieve the desired density, and every interruption of the processing cycle costs money.

Also, changes to the process cycle can only be made by an extensive iterative development process, generally using smaller reactors for test runs, to determine improvements to the "recipe". Unfortunately, once these process improvements have been developed, they must undergo some redevelopment for each reactor and each part geometry they are used with because the manufacturers lack a tool to predict the effect of reactor and component geometry on the standard deposition conditions. These manufacturing problems dramatically increase the cost of CVI-based composites and impede their use in production systems.

Some models for CVI have been developed for the analysis of simple processing systems [1,8,9,10,11], but they are not easily adaptable to the complexity of the commercial processing systems. Also, these models are not commercial codes and, therefore, sufficient support on the use of the models for different applications by industrial users cannot be assumed.

OBJECTIVES

With the current status of technology, the availability of a predictive tool would be extremely beneficial in cutting the time and costs associated with the development and optimization of a new process.

The objective of the study was to construct, execute, and experimentally validate a computer model for isothermal CVI processes. The feasibility of incorporating the model into a commercial CFD code, FIDAP, will be investigated. Enhancements, if necessary, would be documented for further developmental efforts. Model validations will be for a CVI process using methyl trichlorosilane and hydrogen. By obtaining a fundamental understanding of the CVI process through simulation and experimental validation, the goal of combining advanced CFD capabilities with design optimization and sensitivity analysis techniques can be realized.

In this Phase I study, the modeling effort has been focused on a twofold direction :

1. To evaluate the feasibility of incorporating a densification model for the infiltration of chemical vapors within a cloth preform into FIDAP, a general purpose commercial finite element CFD code.
2. To validate the model via comparison with the experimental infiltration results from actual preforms.

Upon completion of the above two objectives, recommendations for future code enhancement and experimental testing necessary to obtain better process and property data can be realized.

Recently CFD codes have become a very successful engineering tool performing a variety of simulations ranging from turbulent flows to conjugate heat and mass transfer problems. They are used both in process simulations and design optimization to gain deeper insight in complex phenomena and ultimately to investigate, in a cost and time effective manner, the effect of modifications of design variables on existing and proposed processes.

One of the most appealing characteristics of general purpose commercial codes is their use by engineers who do not have extensive mathematical and programming experience. These engineers, having both the theoretical and practical background in their disciplines, can exploit the capabilities offered by the simulation tools.

A second and more important advantage of today's codes is their user friendliness which has significantly reduced the time and effort needed to construct the discretized mesh of the physical domain, prepare the input files describing the physics of the processes involved, and effectively post-process results for evaluation. Construction of meshes of complex geometries can be aided by the use of CAD tools that are nowadays a standard in many industries. CFD simulation software offers design engineers a tool, providing results through numerical experiments. The results are analogous to those obtained through physical experimentation but, in most instances, provide greater resolution of the field variables. Through numerical experimentation, an engineer can test various hypothesis, perform sensitivity studies, evaluate the effects of design modifications, and optimize performance

A key issue in the use of every model is the reliability of the results: particularly for complex problems where the physical modeling is the most challenging task. Before the model can be used for the solution of actual problems, it must pass through a validation process where the reliability of the results is established through a careful comparison with experimental data.

MODELING CHEMICAL VAPOR INFILTRATION PROCESSES

The simulation of chemical vapor infiltration (CVI) processes requires a modeling effort which must consider complex interaction between geometrical, physical, and kinetic parameters and which must be transferable to the software and made available to the CVI user community in a time and cost efficient manner. Models characterizing the physics and geometry must be validated whenever possible by comparison with experiments. Evaluation of the results of these comparisons can suggest modifications of the proposed models at early stages of their development.

Chemical vapor deposition (CVD) processes are similar to CVI, except that the deposition occurs on predefined surfaces. CVD processes are already fully within the capabilities of a CFD code and have been used throughout the industry in recent years. The lack of reliable information on kinetics is probably the largest source of uncertainty. Diffusion rates and other physical properties of all the chemical species present in the reactor can usually be obtained from open literature. When diffusion occurs in a porous media, other phenomena need to be taken into account. Diffusion through pores of small radius becomes dominated by Knudsen diffusion rather than occurring as a Fickian process. In CVI processes, the reaction data requires the knowledge of the preform internal surface area which requires a knowledge of the preform architecture.

CVI processes continue to be investigated in order to improve the efficiency which relies on the diffusion of the reactant species into the preform in order for the deposition to occur. The reaction rate is controlled by the reactor temperature which is usually held constant. The principal problem of such a technique is that high reaction rates, which would be desirable for a faster densification, give rise to premature closure of the outer pores. The ratio of diffusion to rate of reaction rate, usually expressed as a function of the Thiele modulus, Φ , cannot exceed a critical value if a premature closure of the external pores has to be avoided.

$$\Phi = \frac{2kL^2}{rD}$$

In the above equation, r , is the effective pore radius, L , is the preform thickness, and k and D are the reaction rate and diffusion coefficient respectively.

The need for more economically viable (i.e. fast) ways to conduct the densification process has suggested different solutions for the infiltration of the reactant species and the operating conditions of the reactor. Some of the possibilities for controlling the actual rate of deposition which have been suggested include densification under thermal gradients, forced flow, and pulsed flow with and without heating [8,9,10,11].

While some process configurations (for example, the classical Oak Ridge National Laboratory model [1,12] with forced flow and thermal gradients) have been extensively tested and have reached the status of commercial viability, others are still at the level of basic research. Some analytical models (or semi-analytical uni-dimensional cases) have been investigated, mainly to prove that the possibilities exist for adapting some of the configurations in such a way that good densification can be obtained within a shorter time interval.

Morrel et al.[8,9,10] have studied the pulsed power process using microwave heating in order to effectively decouple the diffusion phase from the reaction phases and to have an optimum (i.e. inside out) densification. Their conclusion is that the possibility of a uniform densification exists provided that the process operating conditions are properly chosen. Middleman [6,7] and Sheldon [11] have investigated the possibility of obtaining the desired densification via control of the kinetic characteristics of the process. The existence of multiple solutions to the problem of achieving the infiltration with less time and a minimal amount of residual porosity is very encouraging from the point of view of future industrial applications of CVI. The optimal operating point, when shown to exist, is very sensitive to design and process parameters. It is essential that the value of these parameter be known within a certain level of confidence for the process to be properly designed. The lack of accurate property and reaction rate data for practical CVI processes, is probably one of the reasons why the isothermal-diffusion dominated process, despite known disadvantages, is still the dominant one for the industrial production of complex shape preforms.

The literature reviewed describes possible ways the infiltration process can be conducted and clearly shows that the ability of a model to provide reasonable results requires a coupled solution of the equations of flow, energy, and chemical species with volume heating and chemical reactions. Furthermore, it is necessary to describe how these phenomena develop within the preform which can usually be considered as a porous media, and how the interaction between the geometrical characteristics of the fibres, permeability and diffusion of gas flow between fibers, and reaction kinetics

can be used to estimate the change of effective porosity as a function of time. This is certainly the most challenging problem.

The fact that the fibrous preform is considered as a porous media implies that the geometric properties of the preform are described in an average sense. An estimate of "average" properties requires some information about the structure of the preform. Recent work by Melkote and Jensen [5] and Sotirkos and Tomadakis [13] have been devoted to a statistical evaluation of these properties based on a Monte Carlo simulation. Under some simplifying approximations on the geometry of the evolving preform (for example, preforms made of randomly overlapping cylinders), the surface area per unit volume, mean pore radius and also diffusion coefficients can be evaluated as a function of the fiber radius. In these situations, the surface area of the fibers as a function of porosity can also be calculated.

A CFD model can make use of these pore/fiber relationships together with experimental data, when available, in its continuum-wise description of the infiltration phenomena. The term continuum-wise when describing porous media means a statistical description. When the results of the computation are presented in terms of fiber radius or porosity at a certain spatial location, it does not mean that an actual fiber exists at that location, but rather that the average reaction rate and reactant concentration have determined a certain deposition rate as a function of time as predicted by the analysis. This deposition rate can be related to the rate of growth as a function of time of a representative fiber radius.

This kind of description does not constitute a loss of information from an engineering point of view where it would have no meaning to try to describe in detail the densification on a single fiber. On the other hand, it does require care in the interpretation of results. When comparing the simulation results with experimental data, the incremental increase of individual fiber radii should be properly averaged over a large number of fibers. Also, a clear understanding of the structure of the preform is necessary. If information on variations or discontinuities in the actual preform are not made available to the model, the average description will not be able to provide any information as to the effect of these discontinuities on the growth rate.

MODELING AND ANALYSIS

Model Description

As anticipated in the previous section, the description of the CVI process requires a simplified representation of the complex mechanisms that determinate the efficiency of the process. The goal of the current study is not to focus on the details of the process but to evaluate the parametric sensitivity of process parameters such as pressure, and temperature, on the rate of and spatial uniformity of densification within the porous body..

The CFD code, FIDAP, currently has the capability to allow for variations in reactor geometry; reactor heating including element size, shape, and power; preform size and shape; inlet gas flow rate and composition; inlet gas distribution manifolds; reactor wall and deposition surface temperatures, inlet gas temperature and pressure; location of inlets and exits; and internal baffling and reactor insulation.

The isothermal diffusion dominated CVI process has been chosen for initial modeling and code validation. The reason for this choice of isothermal CVI process modeling is partly due to the experimental apparatus available for the simulation validations and partly by modeling considerations. The diffusion dominated process requires the minimum amount of physical parameters for the description of the porous media. For instance, no model for permeability is needed as no flow is assumed to occur within the preform. It is thus easier to understand the detail which is necessary in the model of the preform to adequately reproduce the experimental results. It must be pointed out, however, that in the context of the capabilities of the model, the simulation of other kind of processes, does not present any conceptual difficulty and can be easily incorporated in the code. For instance, forced flow CVI processes (FCVI) and processes which have thermal gradients are within the capability of the code.

Although the general implementation allows the simulation on preforms of arbitrary shape with any chemical reaction specified by the user, the current simulations have been restricted to the study of the infiltration of a cylindrical preform and have specifically referred to the infiltration of a silicon carbide matrix in a preform made of silicon carbide fibers using methyl trichlorosilane and hydrogen.

The chemical reaction leading to the deposition of silicon carbide has been modeled as a single step reaction of methyl trichlorsilane and hydrogen with

the rate of formation of the products being proportional to the concentration of the reactant species. Again, more complex reaction could be implemented, except that the lack of data on kinetic parameters would only add further uncertainties in the results.

The remainder of the report will focus on a brief description of the standard equations of the software code, FIDAP, together with the additional features required to model the infiltration process, sensitivities studies of the thermal simulation of the reactor, a description of the experimental apparatus and experimental cases, and comparisons between experimental and simulation data. Finally, from the comparison of the results between computation and the observed densification patterns, the capabilities and limitations of the model are established and suggestion for future work are drawn.

Following is a brief description of the conservation equations available in the FIDAP code. Only the features relevant to the simulations of a CVI reactor are presented. A comprehensive description of the capabilities of the code can be found in the FIDAP Theory Manual [4].

Momentum Conservation

The application of the principle of conservation of linear momentum to a fluid element leads to the equation

$$\rho \left(\frac{\partial u_i}{\partial t} + u_j u_{i,j} \right) = -p \delta_{ij} + (\mu(u_{i,j} + u_{j,i})), j + \rho f_i \quad (1)$$

where, ρ , is the fluid density, u , the fluid velocity and, f , the body force per unit mass

The constitutive relationship

$$\sigma_{ij} = -p \delta_{ij} + \mu(u_{i,j} + u_{j,i}) \quad (2)$$

has been applied, where the stress tensor, σ , is decomposed in the sum of a pressure and deviatoric term, proportional to shear rate tensor through the dynamic viscosity, μ , where, δ_{ij} , is the Kronecker tensor.

Mass Conservation

The principle of mass conservation for the fluid mixture results in the equation

$$\frac{\partial \rho}{\partial t} + (\rho u_j)_{,j} = 0 \quad (3)$$

In addition, mass conservation applies to the components of a mixture individually. In FIDAP, a mixture of N species is described by $(N-1)$ conservation equation formulated in terms of mass concentration. The N^{th} concentration, c_N , is the species concentration of the carrier fluid, which is linked to the remaining $N-1$ by the relationship

$$c_N = 1 - \sum_{n=1}^{N-1} c_n \quad (4)$$

The carrier fluid can be arbitrarily chosen as any of the species present in the mixture and its properties are the reference properties that are input to the code. The rate of change of mass concentration of a species is due to advection, diffusion and chemical reaction.

$$\rho \left(\frac{\partial}{\partial t} + u_i c_{n,i} \right) = (\rho \alpha_n c_{n,i})_{,i} + q_{cn} + R_n \quad (5)$$

Equation assumes that the mass diffusion is governed primarily by concentration gradients. The diffusion coefficient, α_n , can be made a function of any field variable to account for different diffusion mechanisms. R_n is the chemical reaction rate and q_{cn} , is a general source term.

Unless otherwise stated, concentration will always refer to the mass concentration c_n and not to the molar concentration, denoted with $C_n (\text{mol} / \text{m}^3)$

Conservation of Energy

The principle of conservation of thermal energy is expressed by the equation

$$\rho c_p \left(\frac{\partial T}{\partial t} + u_i T_{,i} \right) = (k T_{,i})_{,i} + H \quad (6)$$

where it is assumed that the heat flux is proportional to the temperature gradient through the thermal conductivity, k , accordingly to Fourier's law.

The heat generation term, H , can consist of several factors, including heat generation due to applied sources and sinks, viscous dissipation chemical reaction, electrical (Joule) heating and participating media radiation.

Equation of State

To complete the specification of the problem it is necessary to add an equation of state which relates density temperature, pressure and species concentration. In a typical situation encountered in a CVI reactor the density varies with temperature and species concentration but is independent of pressure. In this case, the more appropriate representation of the density variation is given by

$$\rho = \rho_0 \frac{[1 - \beta_T(T - T_0)]}{1 + \sum_{n=1}^{N-1} (M_N / M_n - 1)c_n} \quad (7)$$

where, ρ_0 , is the reference density of the carrier fluid

The numerator of the fraction includes the effect of temperature variation with respect to a reference temperature through the volumetric expansion coefficient, β_T . The denominator expresses the variation of density due to the presence of species of different molecular weight, M , consistent with the convention implied by Equation 4

Equation of Evolution of Porosity

The above equations represent a brief summary of standard equations solved by the FIDAP code. In a CVI process, the solution of a dynamic equation for the rate of growth of the fibers is necessary. From this relationship, the , time and space evolution of the local porosity can be evaluated.

Denoting with M_s and ρ_s the molecular mass and density of the deposited solid, the equation for porosity can be written as :

$$\frac{\partial \phi}{\partial t} = - \frac{M_s}{\rho_s} \sum_{l=1}^n v_{nl} R_l \quad (8)$$

where R_l is the rate of reaction per unit volume of composite and v_{nl} is the stoichiometric coefficient of species "n" in the reaction "l". The summation is extended from 1 to the number of reactions contributing to the solid deposition. In the case of a heterogeneous reaction, R_l is expressed as

$$R_l = S_A R_{sl} \quad (9)$$

where, R_{sl} , is the reaction rate per unit surface area and, S_A , is the accessible surface area per unit volume of composite.

The transport equation for species are usually reported in the literature in terms of molar concentration and all the reaction data are given in terms of moles, which is the most convenient form for practical applications. However, as already described, the FIDAP species equations, being conservation equations, are better formulated in terms of mass concentration. For this reason, the input data can be automatically converted into mass concentration within the program using the following equation.

$$R_{nl}^{mass} = M_n \rho^m \prod_{j=1}^{n_l} \left(\frac{1}{M_j} \right)^{n_{jl}} k_{nl}^{mol} \exp \left[-\frac{E_l}{RT} \right] \prod_{j=1}^{n_l} c_j^{v_{jl}} \quad (10)$$

In Equation 10, the suffix "n" is again referred to the species while the suffix "l" refers to the reaction: n_l is the number of species in reaction l, E_l the activation energy of the l'th reaction and $m = \sum_{l=1}^{n_l} v_{nl}$. For a single step reaction that in molar terms would be written as

$$R^{mol} = k^{mol} C \quad (11)$$

the conversion expressed by Equation (10) is simply

$$R^{mass} = k^{mol} c \rho \quad (12)$$

Equation 12 simply expresses that the constant of reaction in terms of mass is equivalent to the constant of reaction in molar terms multiplied by the mixture density.

The dynamic equation for the rate of densification has been formulated in terms of fiber radius, r , rather than porosity. The reason for this is that the surface area per unit volume can be obtained in a more straightforward way

and also a direct comparison with the experimental data is immediately available. When the reaction constant is expressed in molar form, the rate of growth of the fiber radius is given by :

$$\frac{\partial r(x,y,z,t)}{\partial t} = \frac{M_s R_s}{\rho_s} \quad (13)$$

When the reaction constant is referenced by unit mass, the following equation would apply.

$$\frac{\partial r(x,y,z,t)}{\partial t} = \frac{k^{mass}}{\rho_s} c(x,y,z,t) \quad (14)$$

Equation 14 is the equation which is actually implemented in the code to allow the computation of the fiber radius as a field variable. From the knowledge of the fiber radius and the structure of the preform, the surface area per unit volume can be obtained. In the same way the diffusivity can be made a function of porosity through the standard method of input into the FIDAP code when including variable properties. If needed, the same procedure could be applied to all the other variables (permeability, specific heat, conductivity) that are function of the rate of infiltration.

The product $K_m c(x,y,z,t)$, which has dimension of Kg/m^2s , is the reaction rate per unit surface in mass form. The reaction rate which appears on the right hand side of the conservation equation for the reactant species is obtained, as its molar counterpart, multiplying the reaction rate per unit surface by the surface area per unit volume.

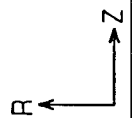
Within the code, Equation 15 is solved as a species equation, canceling the convective term and setting the diffusion coefficient to zero. The dynamic equation is only needed in the preform where the reaction occurs. This region, which is identified as a particular "entity" in the FIDAP nomenclature, is the only one where the rate of growth of the fibers is actually computed. The value of r in the remaining part of the domain, is irrelevant for the computation and is set to zero.

Reactor Simulation

The simplified model, used for the thermal simulation of the reactor is schematically represented in Figure 1 . A quartz tube three inches diameter is surrounded by insulating material and by a dead air space, separating the heating elements from the walls of the reactor and providing temperature

Fig.1 Computational Mesh of Reactor

ELEMENT
MESH PLOT



SCREEN LIMITS
ZMIN - .626E-01
ZMAX .977E+00
RMIN - .429E+00
RMAX .493E+00

FIDAP 7.52
22 Jul 95
18:06:14

control. In this and in all the following simulations, the model is represented as axi-symmetric, taking advantage of the circumferential symmetry of the reactor. The temperature of the heating elements is 900°C while the inlet condition is 20°C. Modeling the reactor as a general 3-D volume does not offer any additional problems.

In the proximity of the inlet and outer boundaries the quartz tube is surrounded by a ring where chilling water is assumed to maintain a temperature of 20°C on the outer wall. All the outer boundaries are assumed to dissipate heat by natural convection. Two different sets of measurements were available for the flow of hydrogen inside the reactor whose operating conditions are listed below. The thermocouple inside the reactor measured a temperature of 900°C, while different temperatures were measured at the outlet sections. These are shown for two experimental conditions in the following table.

Pressure (torr)	Flow (liters/min)	Outlet Temperature (C)
10.9	5	119
7.3	2	83

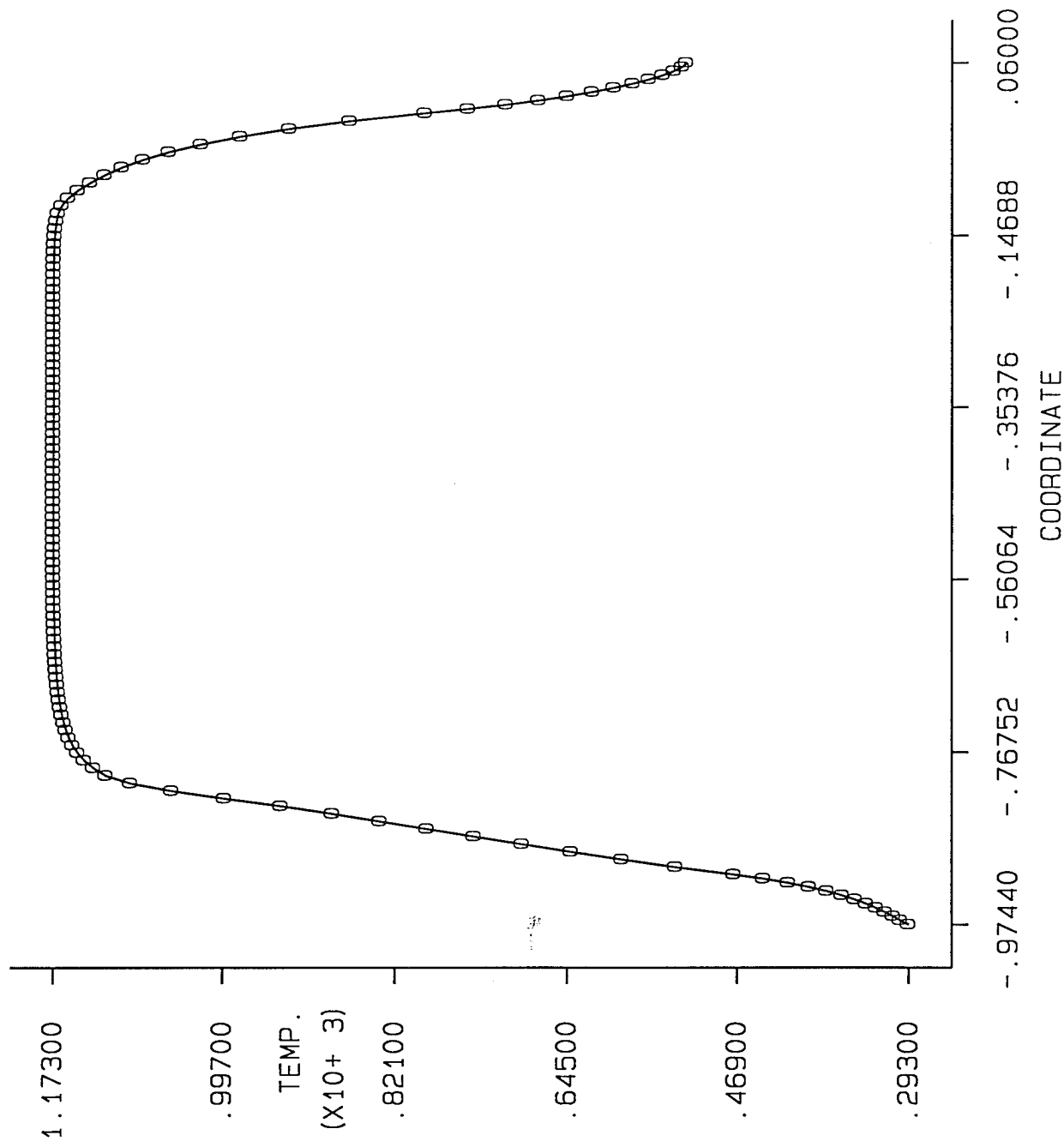
The objective of the simulation has been to compute the temperature distribution inside the quartz tube, in order to verify the hypothesis that infiltration occurs under isothermal conditions. The knowledge of the temperature of the reactor is needed to compute the temperature dependent term in the Arrhenius equation. Due to the exponential variation in Equation 10, it is important to have an accurate determination of temperature.

The temperature variation in Kelvin along the centerline of the reactor is shown in Figures 2 and 3 for the two sets of experimental operating conditions. From these results, it appears that the gas temperature quickly climbs to the control temperature of 900°C (the temperature of the heating elements) and drops rapidly near the outlet. In addition, Figures 4 and 5 show a representative velocity vector field and temperature contours for the first set of experimental conditions given in the above table. This pattern, which matches the experimental observation, is due to the very low heat capacity of the gas. This is a result of the very low density of hydrogen (despite its very high specific heat) at the pressures of 10.9 and 7.3 torr. Also notice that the gradients are much steeper for the case with lower

pressure, causing the fluid to react more quickly to the boundary conditions. Due to the very simplified representation of the reactor, the outlet temperature differs from the experimental value, but this confirms that, for these flow conditions, the temperature in the reactor can be considered isothermal.

In the actual infiltration process, the hydrogen carries the reactant gas (MTS) whose density is much higher than that of hydrogen. In order to verify that the isothermal conditions are maintained in an actual process, the

Fig.2 Centerline Reactor Temperature at Set 1 Cond.



COORDINATE VS.
VARIABLE PLOT

TEMPERATURE

LINE
DEFINITION

POINT

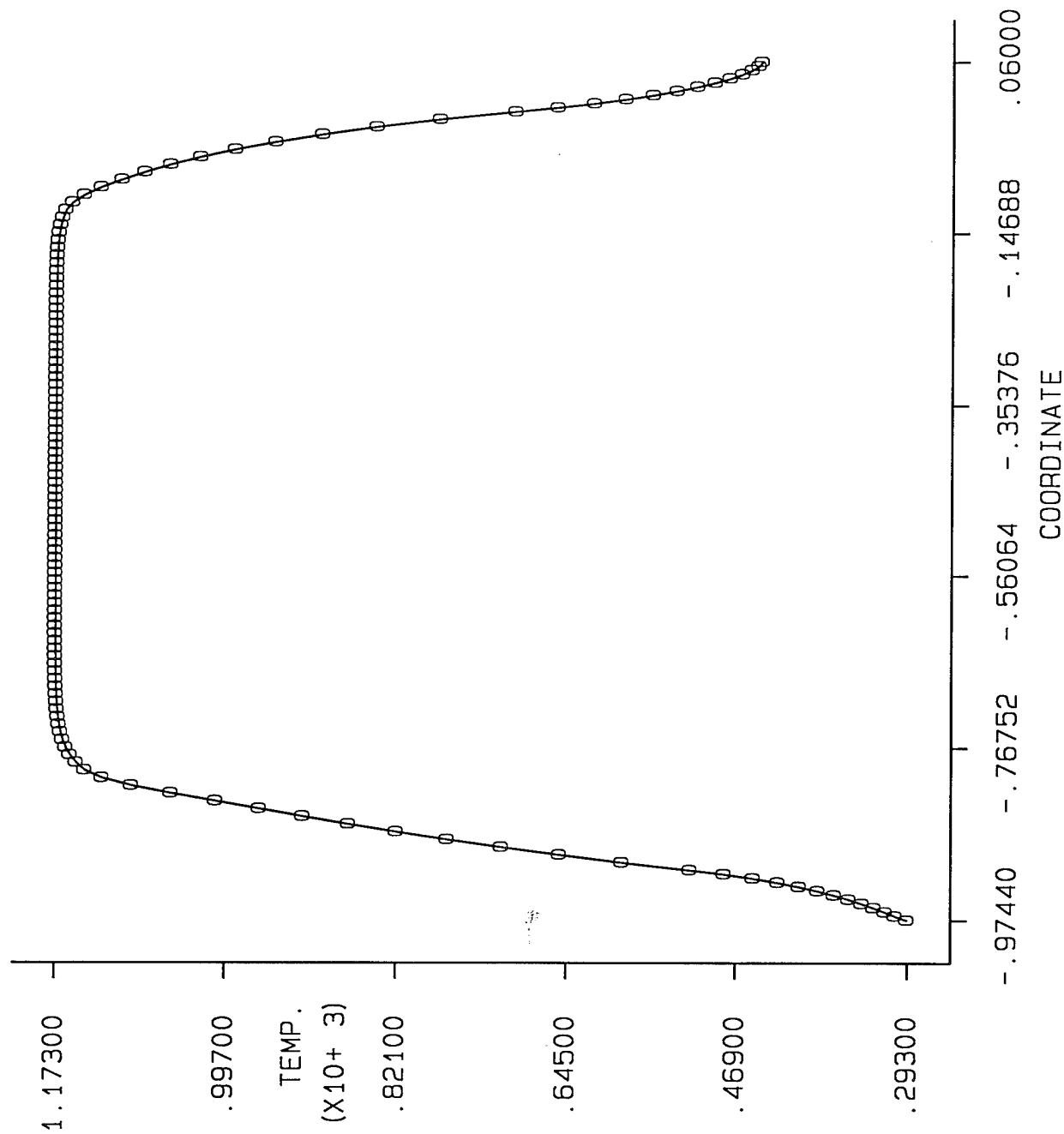
X0 .914E+00
Y0 .366E-01

DIRECTION

X 1.0000
Y .0000

FIDAP 7.52
22 Jul 95
18:08:23

Fig.3 Centerline Reactor Temperature at Set 2 Cond.



COORDINATE VS.
VARIABLE PLOT

TEMPERATURE

LINE
DEFINITION

POINT

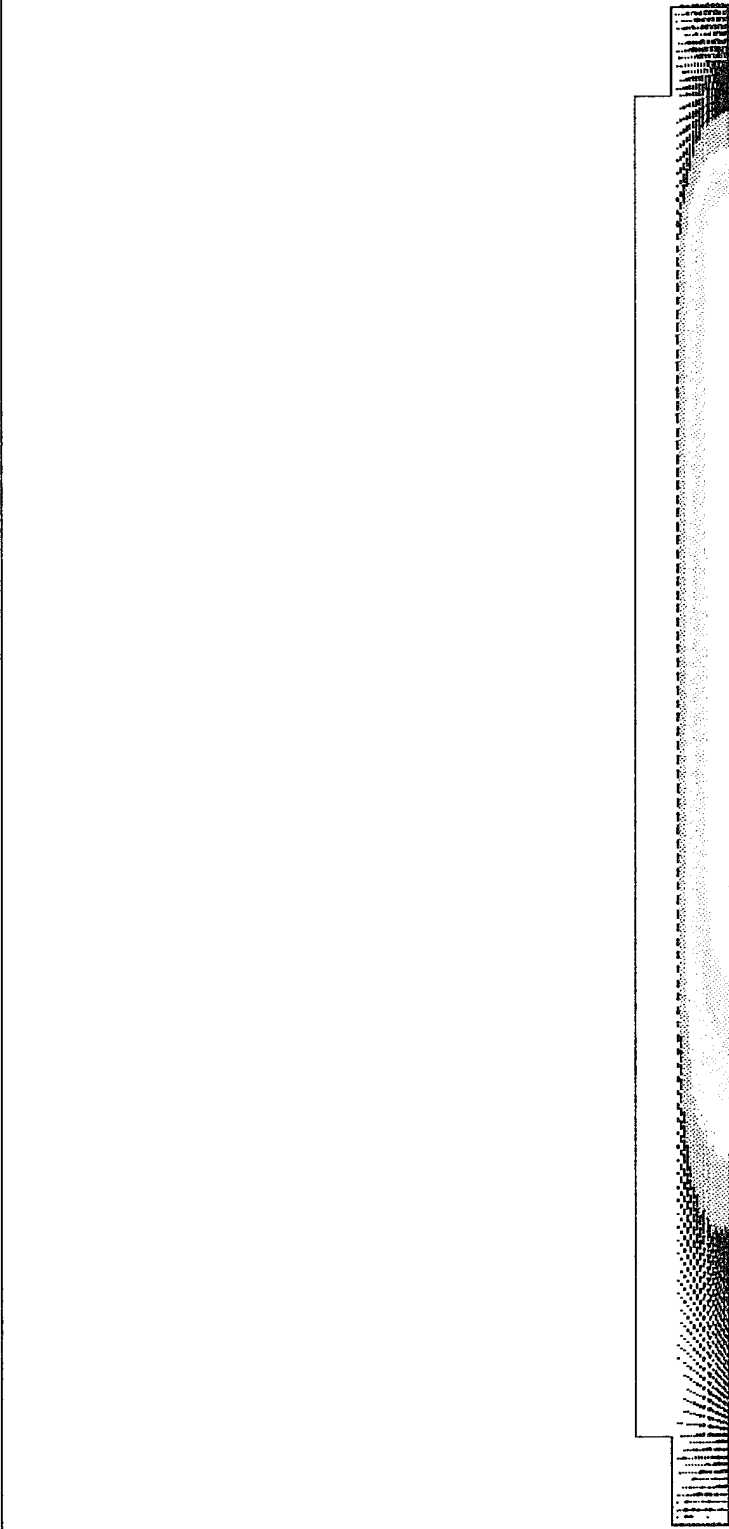
X0 .914E+00
Y0 .366E-01

DIRECTION

X 1.0000
Y .0000

FIDAP 7.52
22 Jul 95
18:10:48

Fig.4 Velocity Field in Reactor at Set 1 Conditions



R
Z

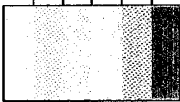
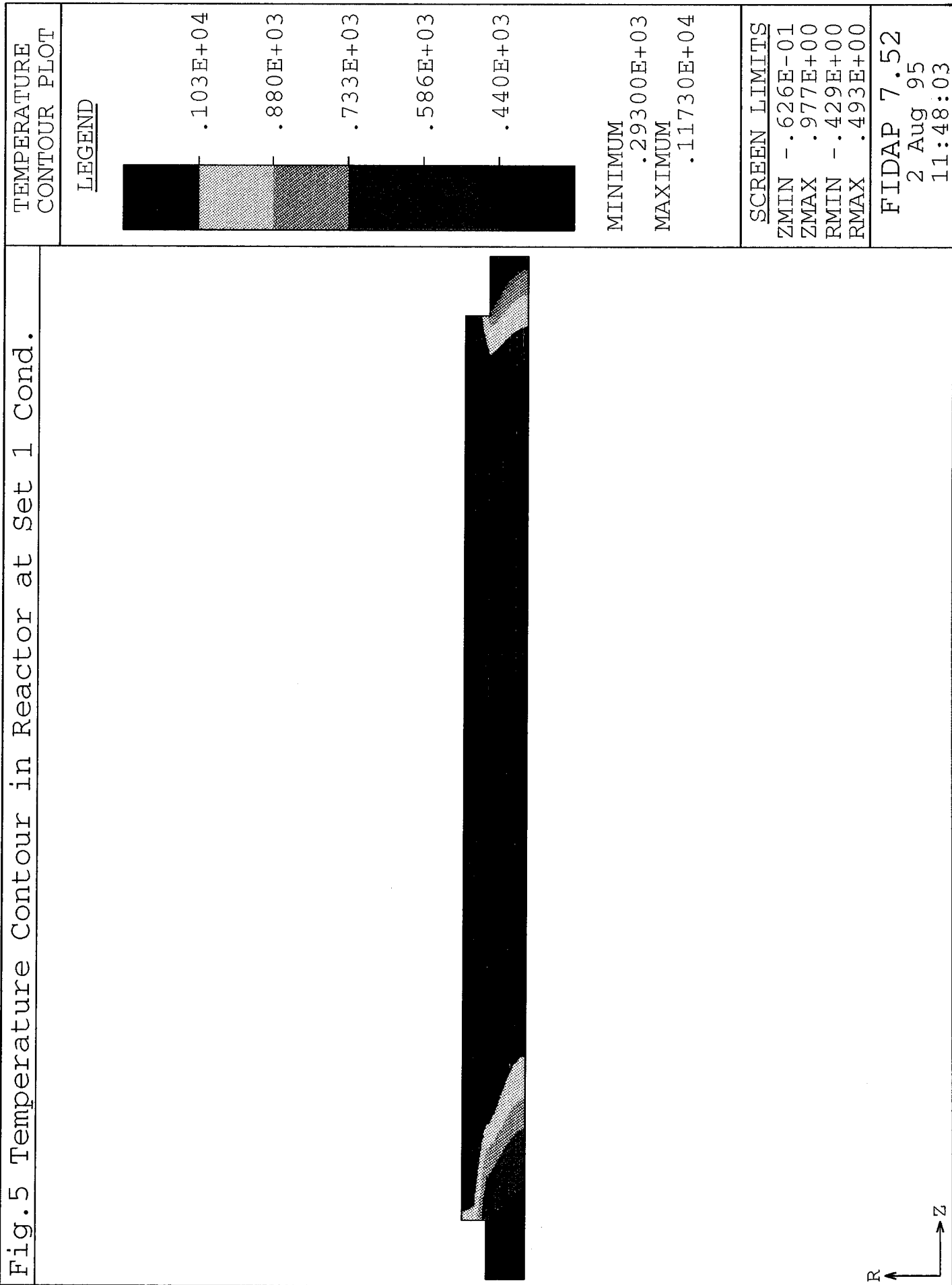
VELOCITY VECTOR PLOT
SCALE FACTOR .5000E+02
REFER. VECTOR → .7688E+02
MAX.VEC.PLOT'D .7688E+02
AT NODE 709
COLOR CODE:
VELOCITY

.641E+02
.513E+02
.384E+02
.256E+02
.128E+02
SCREEN LIMITS
ZMIN -.626E-01
ZMAX .977E+00
RMIN -.429E+00
RMAX .493E+00
FIDAP 7.52
2 Aug 95
11:47:05

Fig.5 Temperature Contour in Reactor at Set 1 Cond.



simulation has been repeated at a pressure of 15 torr (the highest value used during the experiments for the infiltration of the preform), and considering the presence of the reactant gas. The operating pressure of 15 torr results in a higher density gas with a higher heat capacity. The effect of radiation on a solid object positioned inside the tube has also been taken into account.

Figure 6 shows the radial temperature varying along a line intersecting the solid object (preform). The temperature on the solid (left part of the curve) is almost identical to the value of the temperature of the heating elements. Overall, the fluid temperature differs only few degrees from the maximum temperature of the reactor. In summary, the results of the thermal simulations of the reactor confirm the hypothesis of essentially an isothermal reaction thereby allowing investigation of the effects of temperature variations by computing the temperature dependent rate of reaction at the prescribed operating temperature of the heating elements.

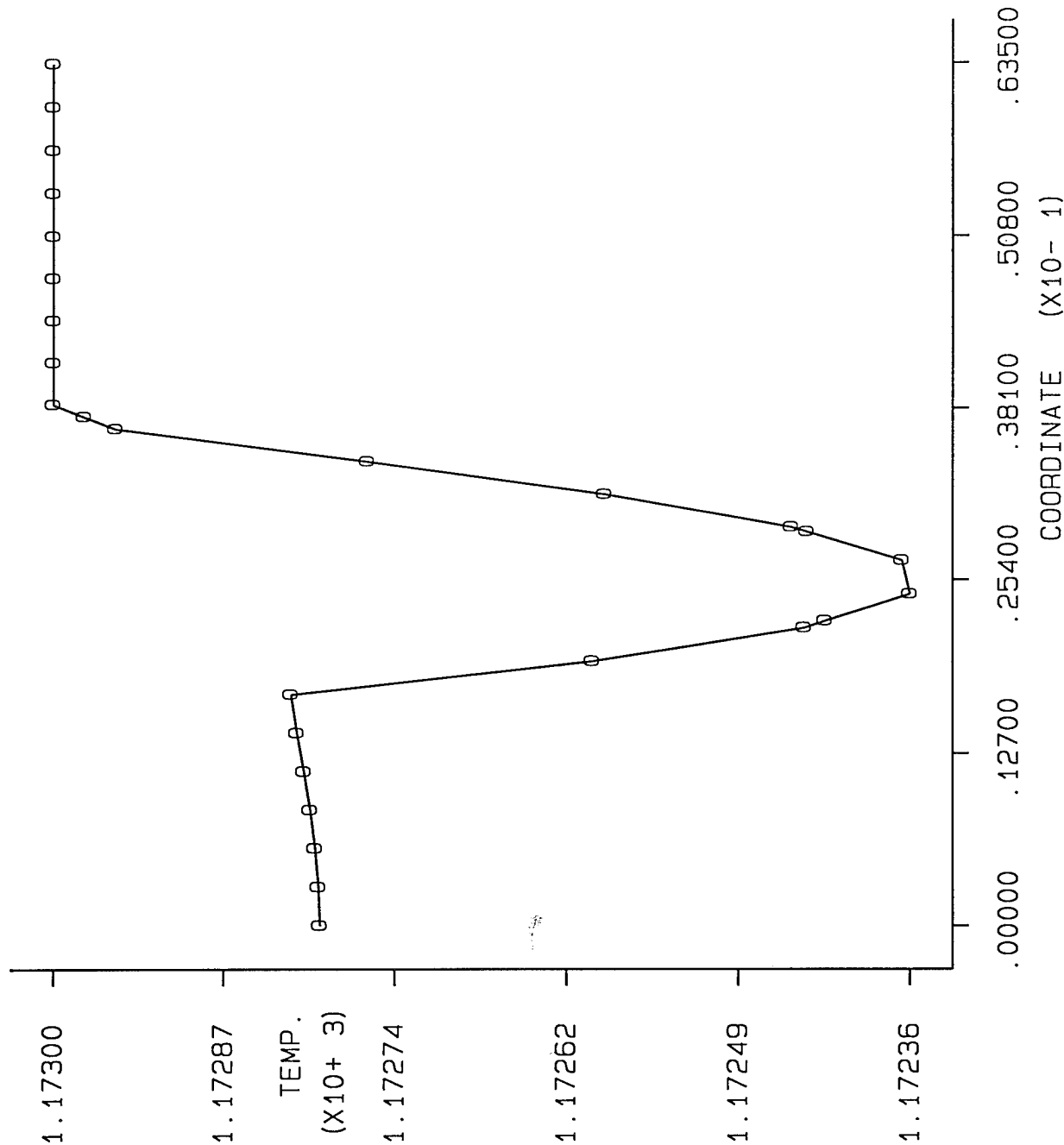
In the global study of the reactor, also the effect of the reaction on the inner wall of the tube has been taken into account in order to compute the distribution of the reactant within the tube. The results of these simulations are used in the model for the infiltration process describes in the following section.

Simulation of the Infiltration Process

The experimental runs of infiltration have been performed on a cylindrical preform of length one inch which is positioned along the centerline of the reactor which is approximately three feet in length. It appears that there is a large difference between the two length scales, with a large part of the reactor not influencing the infiltration process. For this reason, the computational domain has been restricted to a limited part of the reactor containing the preform, which is shown in Figures 7 and 8. The cylindrical preform is in reality a hollow preform but the inner part has been filled with impermeable material and thus is not included in the computation. A zero flux condition is automatically applied by the finite element code at this computational boundary.

The velocity boundary condition at the inlet section has been imposed as a completely developed laminar flow profile. The value of the velocity depends upon the density, which in turn is dictated by temperature and pressure. Accordingly to the results of the previous section the temperature has been set to be the heating element temperature, while the pressure has been fixed to the value indicated by the experimental conditions. Any pressure loss

Fig.6 Radial Temperature Profile at Reactor Mid Height



COORDINATE VS.
VARIABLE PLOT

TEMPERATURE

LINE
DEFINITION

POINT

X0 .460E+00
Y0 .000E+00

DIRECTION

X .0000
Y 1.0000

FIDAP 7.52
25 Jul 95
11:25:03

Fig.7 Computational Mesh With Preform

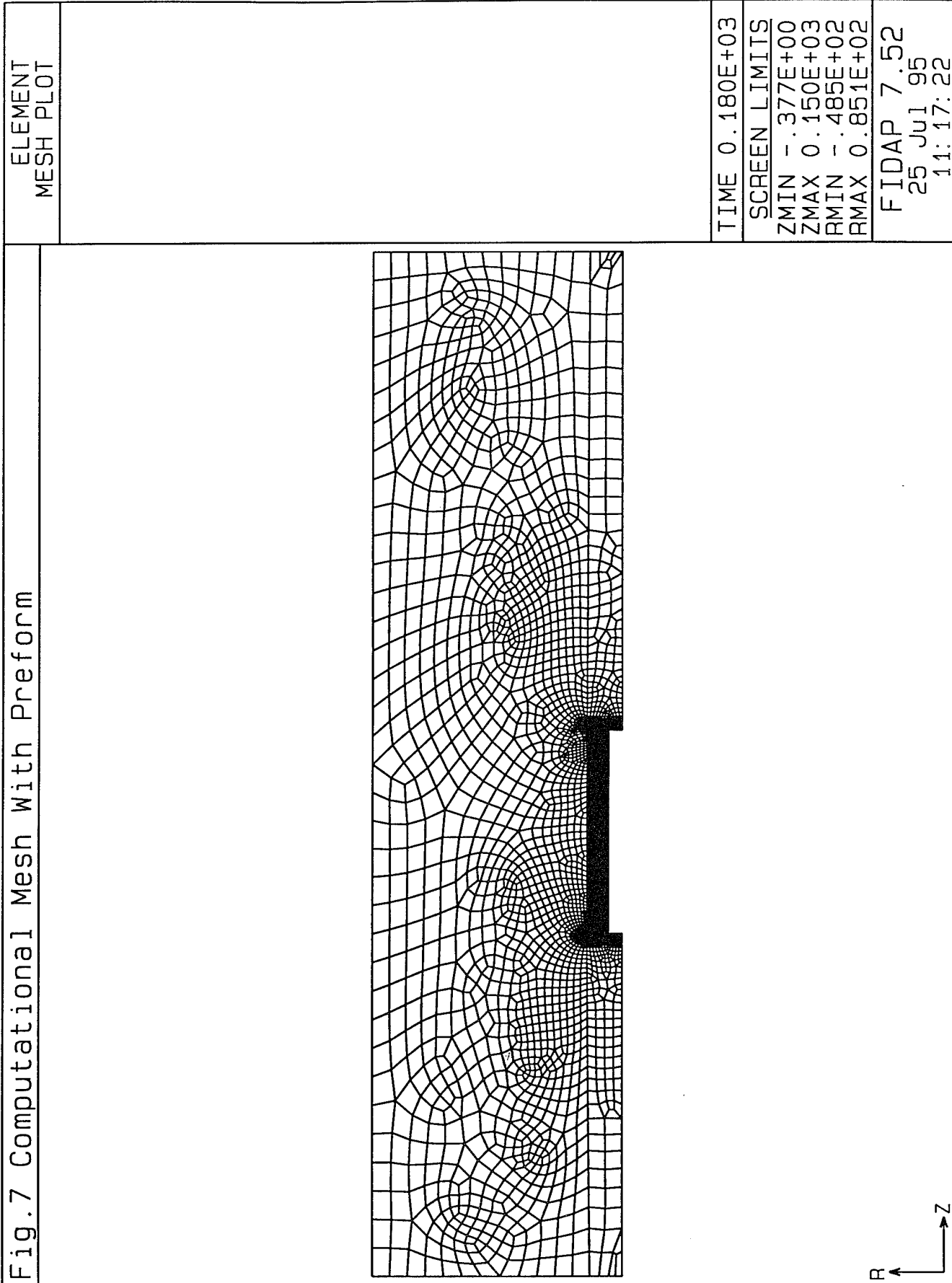
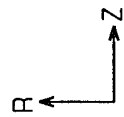
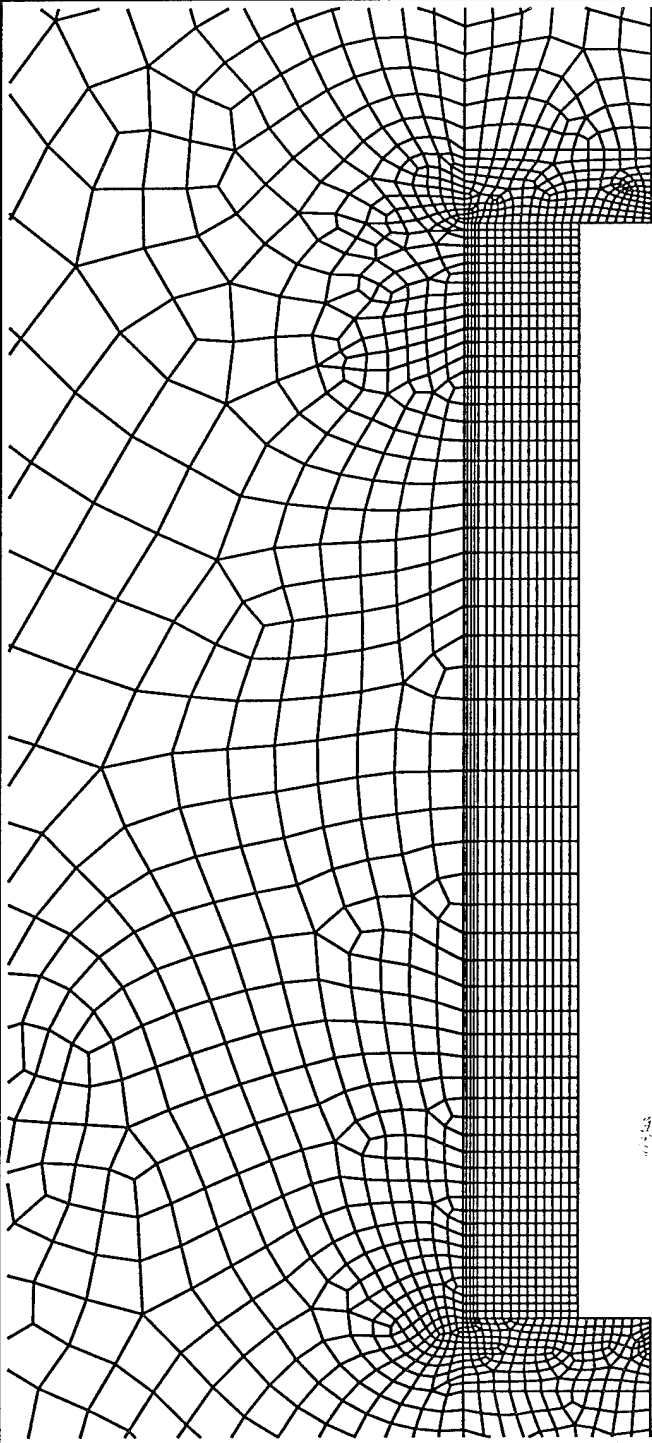


Fig.8 Enlarged View of Computational mesh



ELEMENT
MESH PLOT

TIME 0.000E+00

SCREEN LIMITS

ZMIN 0.467E+02

ZMAX 0.858E+02

RMIN -.169E+02

RMAX 0.178E+02

FIDAP 7.52

2 Aug 95

12:31:25

within the tube is seen to be negligible. Also a parabolic profile has been imposed for the reactant concentration at the inlet section.

In the context of FIDAP simulations, the concentrations are always referred to as mass concentration. The hydrogen is the carrier flow and two species equation are solved for the reactant (MTS) and the product of the reaction. This are referred to as species "1" and "3" in the presentation of the results. The species "2" is solved to track the evolution of the fiber radius at each point of the preform, as explained in the previous section, Equation 13.

Due to the large molecular weight of the MTS compared to the molecular weight of the carrier phase, the mass concentration of the reactant is a number close to unity. The volumetric flow (at normal conditions) is 3.7 liter/min while the mass flow of the reactant gas has been fixed to the value of 3.7 g/min. This translates into an initial value of 0.93 for the mass concentration of the reactant gas. The density is also seen to be a function of the species concentration according to Equation 7.

In the isothermal diffusion dominated infiltration, the only variables needed for the simulation are the reaction data and the diffusivity within the preform. As the decomposition of MTS is modeled as a one step reaction, it is described by an activation energy and a pre-exponential factor. Despite the fact that this hypothesis is widely adopted in the literature the activation energy values are found to vary between 100 and 180 KJ/K-mole. Due to the exponential factor, this uncertainty translates into a much larger uncertainty in the reaction data. (in this range a 50% variation in the activation energy leads to a uncertainty of three order of magnitude in the reaction data).

The value which is most consistently adopted in the literature is 120KJ/K-mole and for this reason it has been adopted in our simulations. The pre-exponential factor has been estimated by comparison with the results from one simulation run at 900°C and 5 torr. The value which was been computed is 4.0 m/s, which is about 50% larger than the one estimated by Morrel et al. [10] with the same activation energy on the basis of the experimental results of Brennfleck, et. al. [3]. Both of these values are obviously kept constant in the parametric studies.

As already pointed out in the introductory section, the adequate description of the structure of the porous media is the most challenging and complex part of the simulation of CVI. The actual structure of the preform is described in more detail in the experimental section. An axial section of the preform reveals that it is comprised of large tows (numbering 3-4 in the radial

direction) that include the fibers to be coated. The tows are also separated by large spaces where the gas is free to flow.

It appears evident that such a structure significantly differs from the "random overlapping cylinders" for which some relationship between pore radius, surface area per unit volume and diffusivity have been obtained [5,13]. The densification process will pass through two different stages; the first when coating is within the tows, and secondly, when the outer surfaces of the tows are sealed. Further deposition within a tow is unlikely.

In an axi-symmetric model, which assumes circumferential symmetry, a detailed description of the structure of the preform cannot be incorporated. When Equation 15 is solved to determine the rate of growth of the fiber radius at each location of the computational domain, there is no capability to determine if that location is occupied by a tow or by free space.

The implications resulting from a lack of information about the structure of the preform are as follows. The presence of large spaces between the tows suggests that the initial diffusivity to be used in the model can be the binary diffusivity of MTS in hydrogen ($2.2 \text{ cm}^2/\text{s}$). This value is then linearly decreased with the growth of the fiber radius to account for the fact that despite the presence of free spaces the "free path" for the reactant is progressively reduced. The difference between the rate of growth of the fiber radius between the surface of a tow and its inner part cannot be adequately described by this model as it not able to selectively reduce the diffusivity in the region of the preform which is actually occupied by the tows.

The results of the simulation thus represent an average rate of growth at each point in space, but, as will appear from the comparison with the experiments, in the range of operating conditions and infiltration times that have been investigated, even a simplified model is able to predict trends and pattern that match the experimental results which also suffer the problem of extracting "consistent" fiber densification patterns from a highly irregular structure.

For different kinds of infiltration process (for example a more rapid process) or for infiltration times that are longer than the ones that have been currently investigated, a more detailed description of the preform, able to represent both the tow and fiber scales, becomes certainly crucial for correct prediction of the densification pattern. In the context of the current model that is implemented within FIDAP code, this would translate into a three dimensional representation of the preform architecture with the to

distinguish different situations for the modeling of diffusion and surface area within the preform.

EXPERIMENTAL STUDY

The Phase I experimental objective was to perform selected CVI experiments on NicalonTM 3D-braided preforms and gather data on deposition profiles to determine the abilities or accuracy of the baseline version of FIDAP. The intent here is not to determine optimum conditions for infiltration but rather design experiments to test the FIDAP model for predicting deposition trends. In order to test the sensitivity of the FIDAP model, an experimental plan was outlined to perform deposition runs over a narrow range of temperatures and pressures. A set of experimental conditions were selected from previously published work [2]. Depositions were carried out at temperatures of 880°C, 900°C, and 920°C and pressures of either approximately 5 or 15 torr. The designed experiments consisted of one long run (35 hours) and several short runs (six to eight hours each). Deposition profiles for the long run were obtained intermittently to determine the deposition rate as a function of time. Initially, several trial runs were made to confirm phase pure deposition of SiC over the length of the reactor. The deposits appeared to be dense and smooth with x-ray diffraction data showing phase pure SiC. No effort was made to identify the exact polytypic modification of SiC. The deposition runs were carried out on a tubular NicalonTM 3D-braided preform in a hot-wall CVI reactor.

While the experimental results obtained in this study was useful in testing FIDAP's predictive capability, the data was not accurate enough to make critical comparisons between deposition profiles obtained for the various reaction conditions. Several factors contributed to this situation. First, it was recognized that cutting small sections of the preform from the initial stock results in significant fiber spreading at the ends. Hence, for small sample sizes used(0.5 to 1 inch), fiber spreading introduced significant variability in the fiber architecture between each sample. Second, the porous nature of the coated preform caused significant chipping of fibers during sample polishing which caused difficulties in making accurate thickness measurements. Third, due to the build up of MTS byproducts in the exhaust, minor fluctuations were observed in the total pressure of the reactor (2-4 torr) such that critically comparing deposition profiles over pressure domains within 10 torr may not be meaningful.



Figure 9. Optical Micrograph of the 3D-Braided NicalonTM Preform in cross section (magnification 7x)

Figure 9 is an optical micrograph of a cross-section of the preform. The fiber volume fraction of the preform is about 35%. The pore structure of the preform is quite complex with varying pore sizes and geometries. Small pores (less than 3-4 microns) exist between fibers within a tow, fairly large pores (tens of microns) exist between tows within a bundle (3 to 4 tows), and very large pores (hundreds of microns) exist between the various bundles of the preform. In cross-section, the preform wall consists of 3 to 4 bundles of tows.

A schematic of the reactor configuration is shown in Figure 10. Although the schematic does not show all the details of the set up, precise measurements of the various parts of the three-zone furnace including locations of heating elements and thermocouples, inlet geometry, and exhaust set-up were made. This information was incorporated into the model to simulate the gas dynamics in the system. In order to establish boundary conditions for the CVI model, temperature measurements were taken at regular locations within the reactor at a set temperature of 900°C while flowing 5 liters of hydrogen gas. The measured temperatures in the hot zone were within 2°C of the set temperature. Results obtained from model simulations of these blank runs is presented in a following section.

The preforms were supported by passing a Ni-Cr wire through the annular gap and placed at the center of the reactor. Special care was taken to ensure that the preform was placed axisymmetrically at or near the same location for all the runs. It was assumed that gas transport through the annular gap of the preform was negligible because of its small i.d. and the metal wire support that was inserted through it. Methyl trichlorosilane (MTS) and hydrogen were used as precursor gases for the deposition. The flow rate of MTS was controlled using a peristaltic pump and a weighing balance was used to monitor the mass flow into the flash evaporator. The flash evaporator was maintained at 150°C, and Hydrogen was used as the carrier gas. The volumetric ratio of hydrogen to MTS was maintained at about 7:1 for all the runs. The exhaust was configured with a liquid nitrogen cold trap to collect the unreacted MTS and other condensable byproducts. A capacitance manometer (MKS Baratron Type 122A) was placed at the top of the reactor to monitor the total pressure of the system.

The aim of this feasibility study was to perform several CVI experiments under varying conditions of temperature and pressure and subsequently verify the deposition profiles with model predictions. Infiltrated samples were vacuum cast in epoxy resin, and after curing the epoxy polished to one-micron finish using diamond paste. Deposition profiles in the preform were

characterized by SEM analysis. Thickness measurements were made by SEM and optical microscopy from three sets of tows; an outermost tow, a middle tow, and an inner tow. For each tow, at least ten independent measurements were made on outer and inner fibers. Figure 11 is a schematic representation of the preform with labels designated for the various tows and fibers.

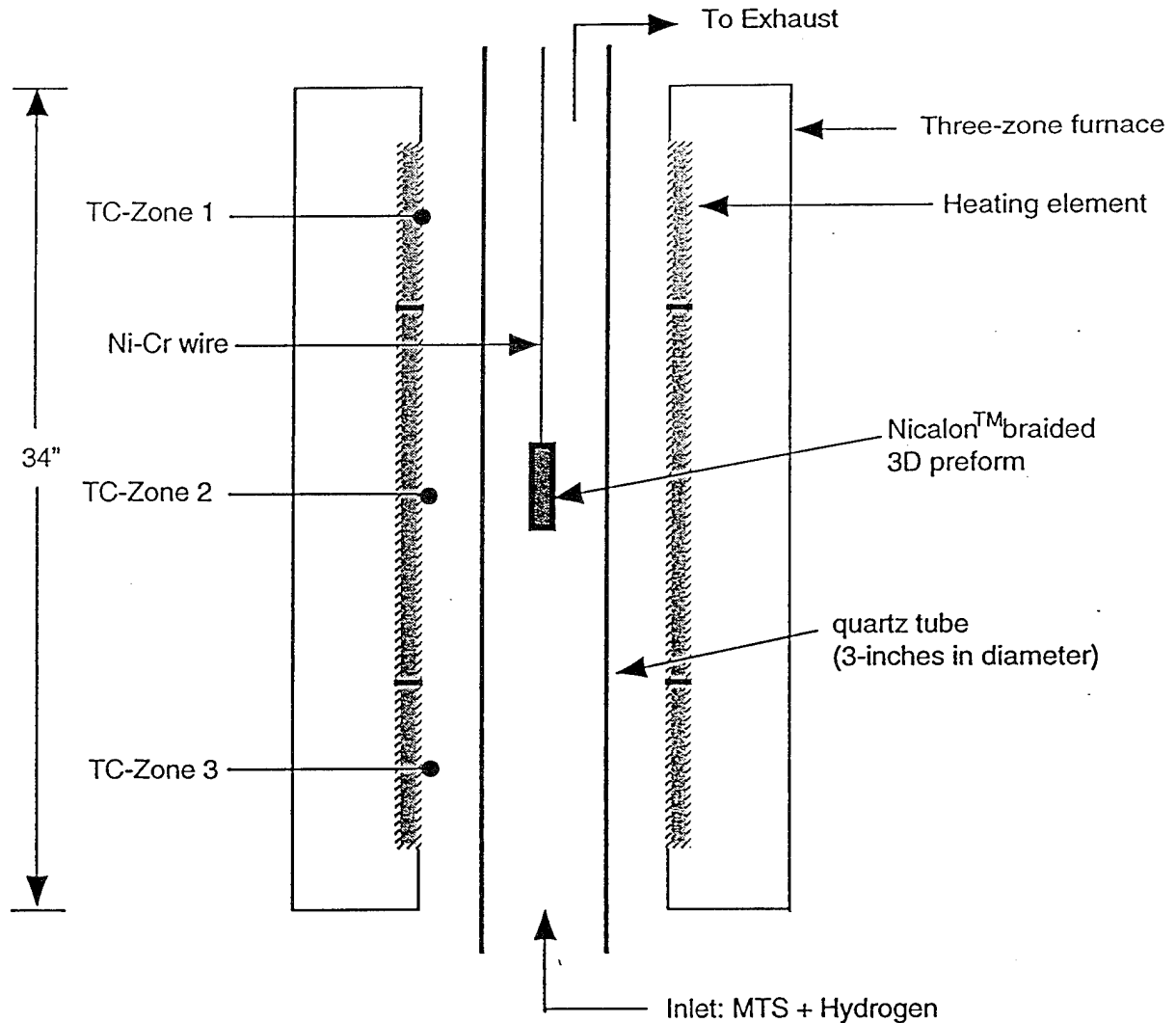


Figure 10 Schematic diagram of CVI reactor

A schematic of the reactor configuration is shown in Figure 10. Although the schematic does not show all the details of the set up, precise measurements of the various parts of the three-zone furnace including locations of heating elements and thermocouples, inlet geometry, and exhaust set-up. All this information was incorporated into the model so that the gas dynamics can be simulated as accurately as possible. In order to establish boundary conditions for the CVI model, temperature measurements were taken from various locations within the reactor at a set temperature of 900°C while flowing 5 liters of hydrogen gas. The measured temperatures in the hot zone were within 2°C of the set temperature. Results obtained from numerical simulations of the two test runs were presented in the previous section.

The preforms were supported by passing a Ni-Cr wire through the annular gap and placed at the center of the reactor. Special care was taken to ensure that the preform was placed axisymmetrically at or near the same location for all the runs. Methyl trichlorosilane (MTS) was used as the precursor while hydrogen was used as the diluent gas. Flow rate of MTS was controlled using a peristaltic pump and monitored through a weighing balance. Hydrogen was passed through the MTS-containing flash pot maintained at 150°C. The volumetric ratio of hydrogen to MTS was maintained constant at about 7:1 for all the runs. The exhaust was configured with a liquid nitrogen cold trap to collect the unreacted MTS and other condensable by-products. A baratron was placed at the top of the reactor to monitor the total pressure of the system.

Deposition profiles in the preform were characterized by SEM analysis. Samples were mounted in epoxy resin and polished to one-micron finish using diamond paste. Thickness measurements were made from three sets of tows; an outermost tow, a middle tow, and an inner tow. For each tow, at least ten independent measurements were made on outer and inner fibers. Figure 11 is a schematic representation of the preform with labels designated for the various tows and fibers. These definitions are utilized in the tables presented in the section on experimental and numerical results.

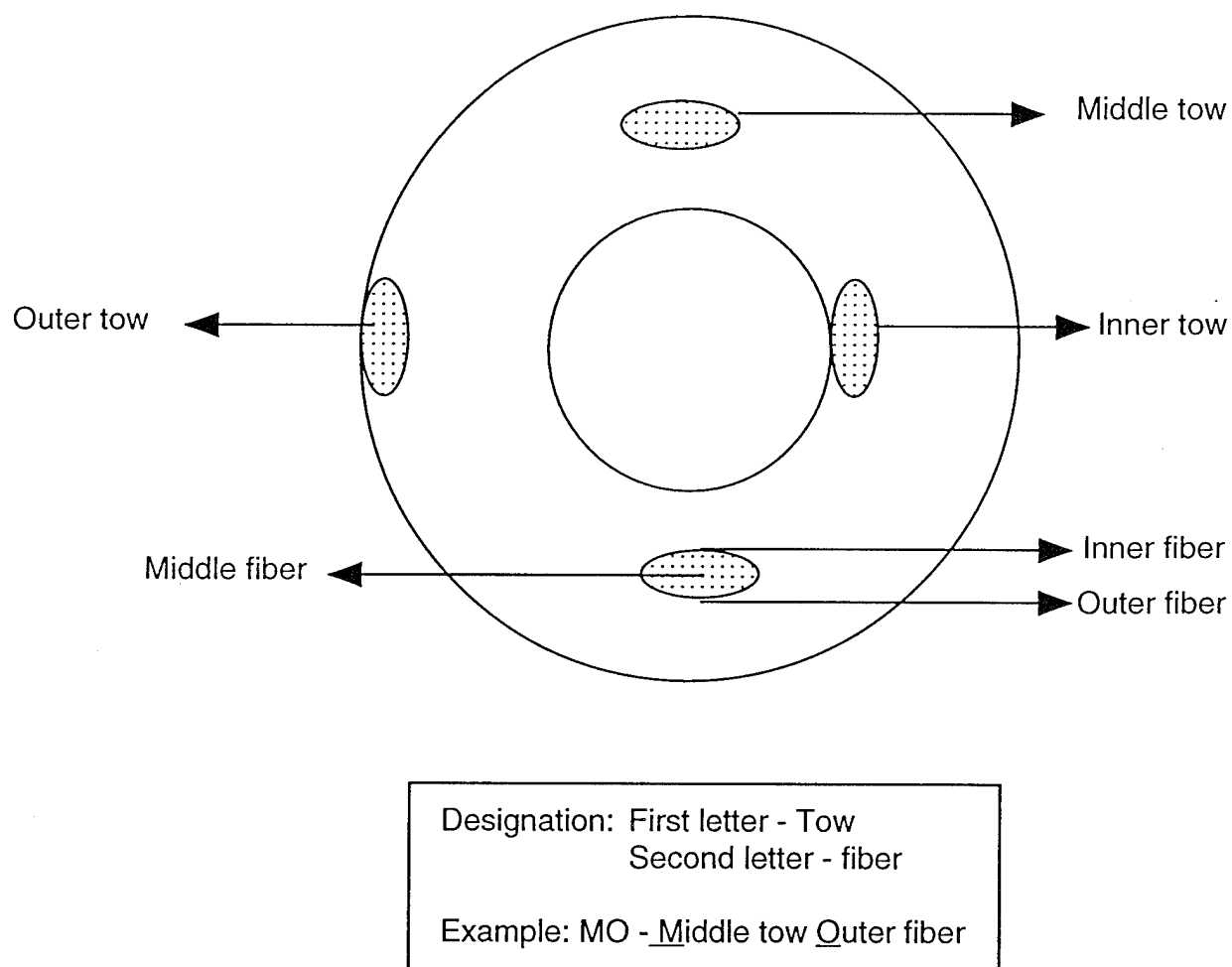


Figure 11. Areas of Characterization Within the Preform.

RESULTS

Experimental Results

Infiltration of the preform was obtained in all cases, however, the uniformity of the deposits varied depending on the reaction conditions. Three sets of experimental results were compiled to compare with model predictions. Table 1 lists the thickness distribution for temperatures of 900°C and 920°C at constant pressure (approximately 5 torr). Figure 12 shows the corresponding optical micrographs of the deposits at the two temperatures.

In CVI processes, use of higher temperatures typically result in thicker deposits on the outer fibers of exterior tows and consequently, due to a decrease in time for diffusion and precursor depletion, thinner deposits on the interior tows. Thus, beyond an optimum deposition temperature, higher temperatures will lead to larger gradient in coating thickness from the exterior to the interior of the preform.

In the present comparison, thickness values on the OO fibers for both temperatures shown in Table 1 appear to be close suggesting very little influence of an increase in temperature from 900°C to 920°C on the deposition rate. However, the thickness profiles for the inner and middle tows appear to be more uniform for the higher temperature run. It is questionable whether this is a real effect due to an increase in temperature or some other geometrical or experimental artifact. For example, since short sections of preform were used, the fiber volume fraction varied somewhat between samples. It must also be noted that the comparisons being made between two preform samples are representative of general locations in the preform and not the exact geometrical location. Therefore, critical assessment of deposition profiles cannot be made based on these results.

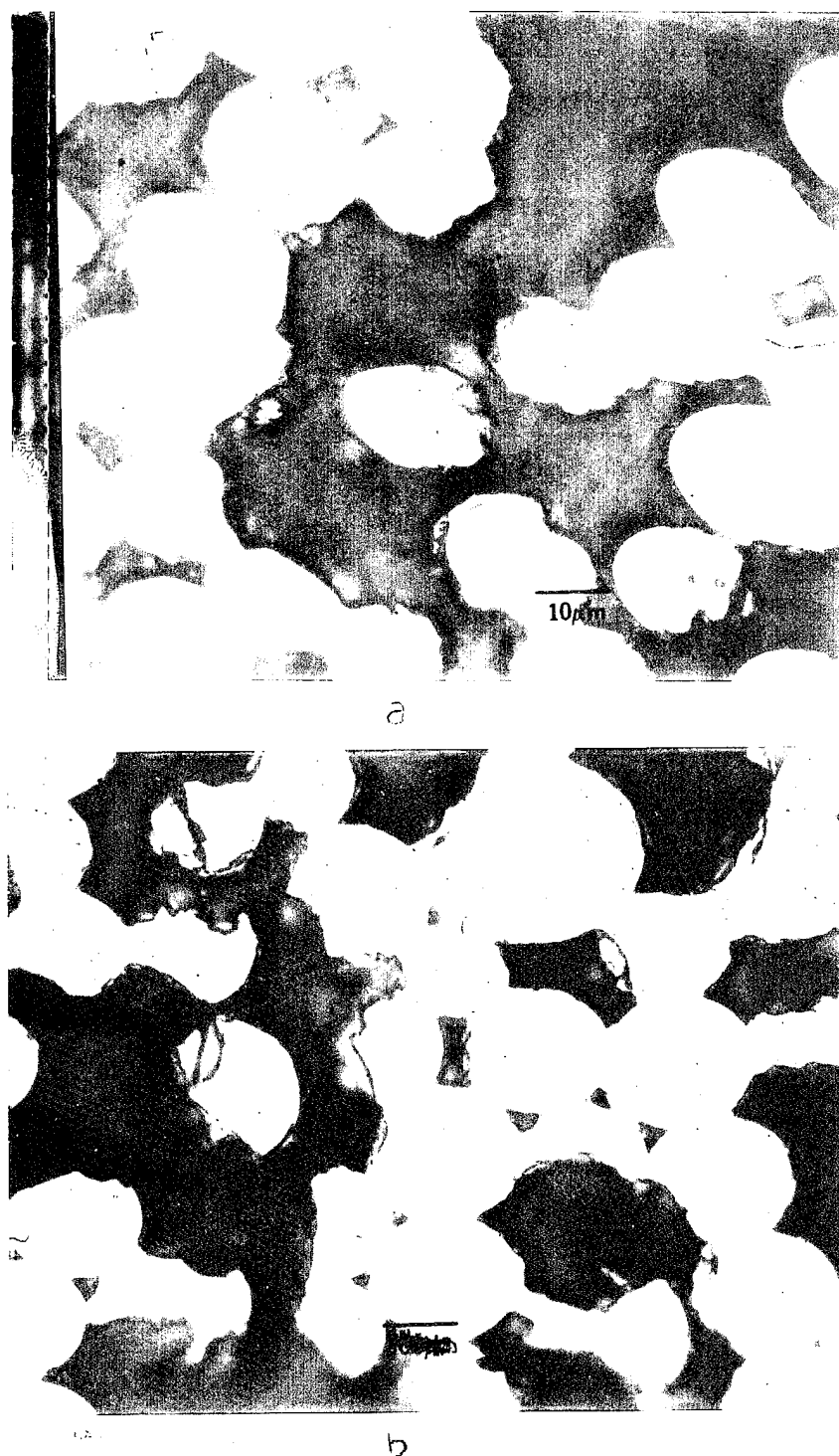


Figure 12 Optical micrographs of II fibers in cross-section at
a) 900°C
b) 920°C

<i>Thickness in microns with s.d. in parenthesis; P=4-5.8 torr, t = 8 hours</i>		
Fiber	900°C	920°C
I I	0.47 (0.12)	0.75 (0.21)
I M	-----	0.80 (0.12)
I O	0.77 (0.08)	0.79 (0.18)
O I	1.39 (0.23)	0.91 (0.13)
O M	0.7 (0.18)	1.48 (0.34)
O O	1.31 (0.24)	1.24 (0.34)
M I	-----	0.80 (0.14)
M O	0.94 (0.11)	-----

Table 1 Thickness distribution as a function of temperature

Table 2 shows the thickness distribution for conditions at pressures of approximately 5 torr and 16 torr and a constant temperature of 900°C. Figure 13 shows the corresponding optical micrographs for the two samples. The higher pressure run clearly shows a significant increase in thickness throughout the preform. This distribution also suggests that an increase in the total gas pressure by 10 torr has a more pronounced effect on the deposition rate than an increase in temperature by 20°C. Furthermore, the distribution at the higher pressure regime also appear to be more uniform. Besmann et. al recently reported an anomalous increase in deposition rate as a function of decrease in total reactor pressure with a maximum occurring at about 2.7 kPa (20 torr) [2]. They relate the higher growth rates to direct decomposition of MTS to SiC which apparently occurs at low pressures rather than formation of intermediate silicon-containing species occurring at higher pressures. Their experimental results show the deposition rate going through an anomalous hike around 20 torr and then falling back to lower values at higher pressures. The higher deposition rate observed in this study was also in the same pressure range (15-17 torr). The coating uniformity obtained under these conditions is somewhat puzzling. One possibility is that this is a real effect rather than a geometrical or an experimental artifact. The

other possibility is that the experiment was not run long enough to scale-up the coating thickness for a better test of uniformity.

Yet another possibility is that, at these low pressures, the gas permeability is relatively high such that uniform infiltration is obtainable. Further work is necessary to fully characterize these effects. It may be worthwhile to pursue infiltration experiments in this pressure range to further optimize the deposition conditions such that both uniformity and high deposition rates can be achieved at the same time.

<i>Thickness in microns with s.d. in paranthesis T= 900 °C, t = 8 hours</i>		
Fiber	4-4.2 torr	15-16.2 torr
I I	0.47 (0.12)	1.02 (0.15)
I M	-----	1.44 (0.20)
I O	0.77 (0.08)	1.38 (0.27)
O I	1.39 (0.23)	1.36 (0.22)
O M	0.7 (0.18)	1.41 (0.34)
O O	1.31 (0.24)	2.18 (0.31)
M I	-----	1.34 (0.15)
M O	0.94 (0.11)	1.94 (0.12)

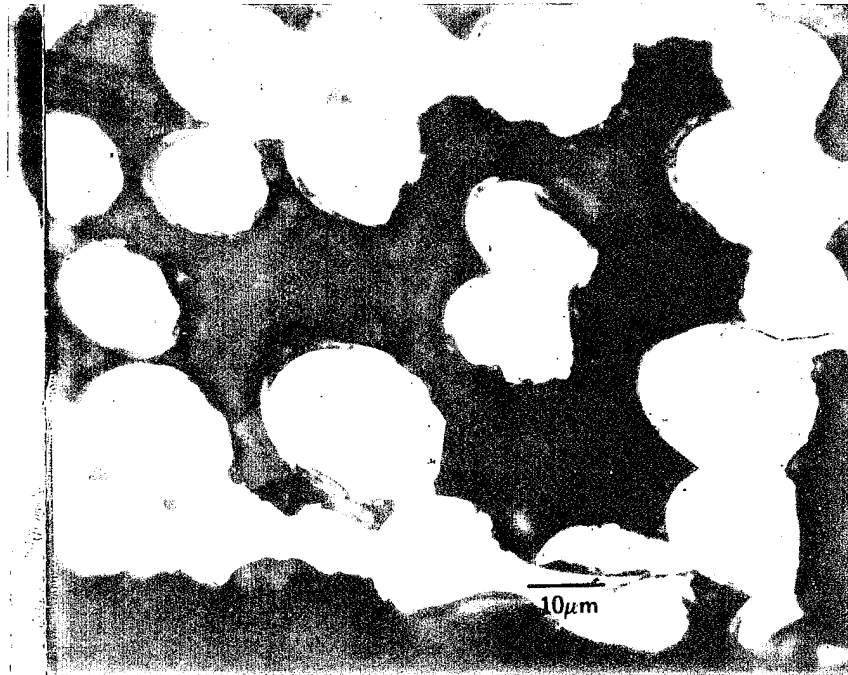
Table 2 Thickness distribution as a function of pressure.

A third set of experiments were carried out to study the deposition of SiC as a function of time at 900°C, 5 torr (see Table 3). Figure 14 shows the corresponding optical micrographs for the two samples. This run was carried out for a processing time of 35 hr. through a total of seven runs. Initially, a sufficiently long preform was used to allow for cutting a sample after each run segment. The purpose of these experiments was to monitor the deposition profile as a function of time and to be able to identify the time at which the outer scale formed, which would have prevented any further infiltration. Unfortunately, sufficient data is not available to be able to identify the

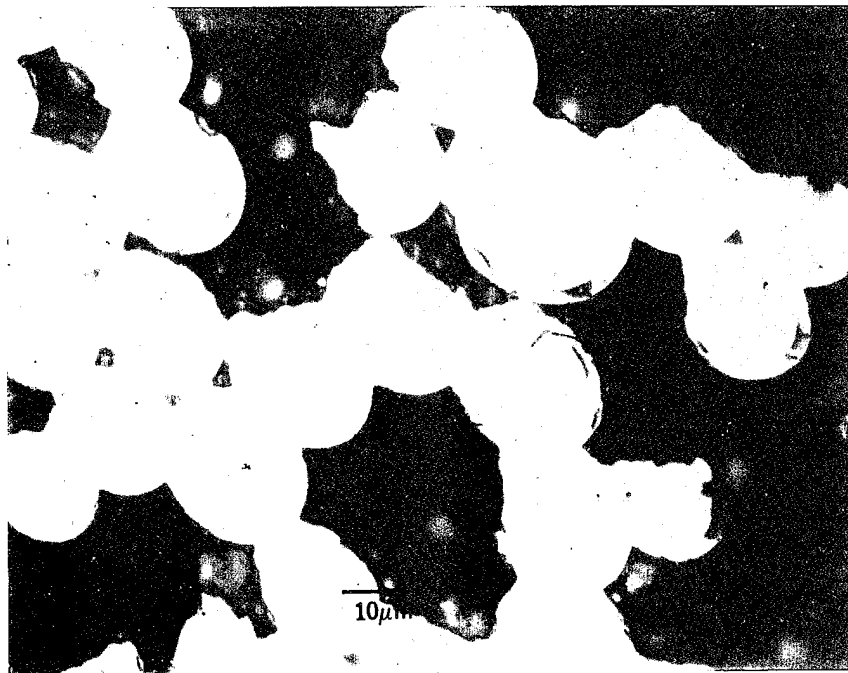
precise time at which the scale was formed. However, the scale formation can be clearly seen at the end of the 35-hour experiment (Figure 14A).

Based on the data given in Table 3, a rough estimate for the scaling time can be calculated. Scaling seems to have occurred at different times for different tows. Once an impervious outer scale is formed, any further growth will occur only on OO fibers. Based on the data given and assuming a linear growth rate, the approximate rate at which the growth may have stopped for each of the inner fibers can be calculated. It is obvious from the distribution given that the results are inconsistent. For example, The OI fibers show no growth after the 8 hour run while the OM fibers show growth over a period of 24 hours. It is difficult to analyze these results because different tows scaled over different times. This behavior would be expected for non-optimized CVI processes.

The partial scaling of tows would have allowed deposition only within open bundles. Further experimentation is necessary to fully characterize the evolution of the densification process.

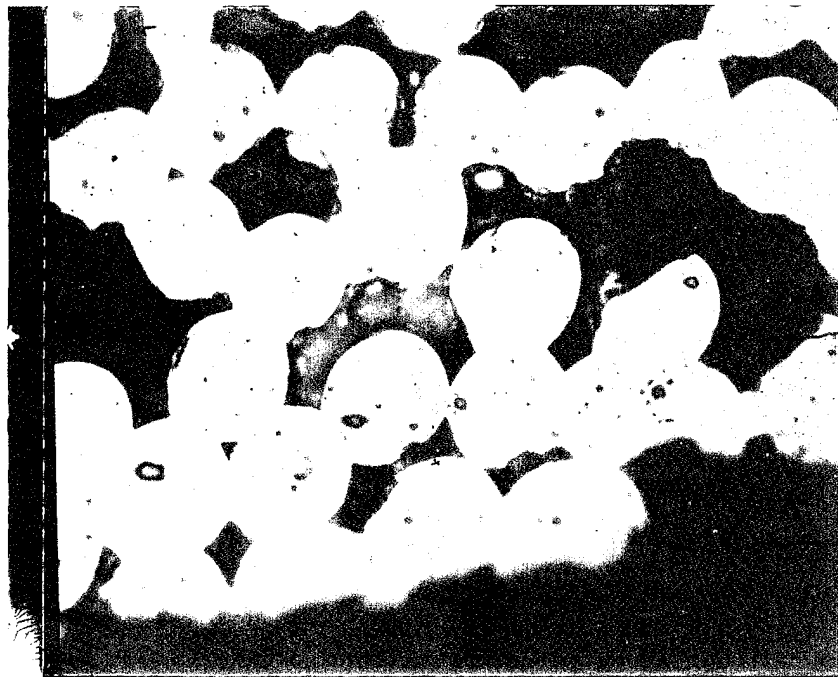


(a)

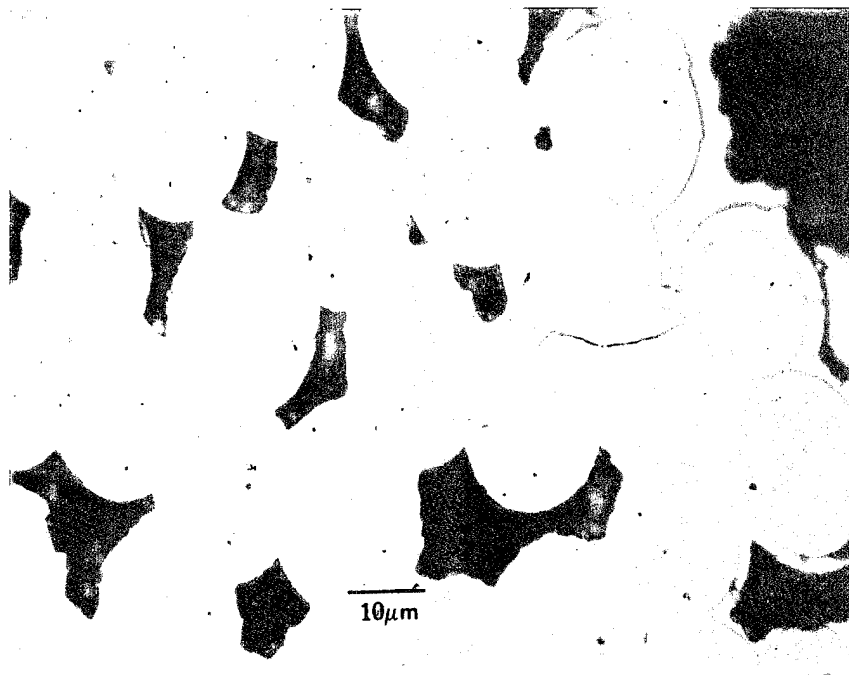


(b)

Figure 13. Optical micrographs of MM fibers in cross-section at
a) 4-6 torr
b) 15-17 torr



a



b

Figure 14 Optical micrographs of OO fibers cross-section at 900°C for
a) 8 hours
b) 35 hours

<i>Thickness in microns with s.d. in paranthesis $T = 900^{\circ}\text{C}$, $P = 4-4.2$ torr</i>		
Fiber	8 hours	35 hours
I I	0.47 (0.12)	1.49 (0.50)
I M	-----	0.84 (0.22)
I O	0.77 (0.08)	1.84 (0.33)
O I	1.39 (0.23)	1.32 (0.41)
O M	0.7 (0.18)	2.10 (0.55)
O O	1.31 (0.24)	2.87 (0.73)
M I	-----	1.01 (0.28)
M O	0.94 (0.11)	2.10 (0.47)

Table 3 Thickness distribution as a function of time



Figure 14A SEM micrograph of the preform after 35 hours

Computational Results

Figures 15 through 22 show results of the numerical simulations. In the computational results the rate of densification is expressed through the spatial and temporal variation of the fiber radius, starting from its initial value of 5 microns. In order to obtain the rate of growth which has to be compared with the experimental data this initial value has to be subtracted from the actual fiber radius.

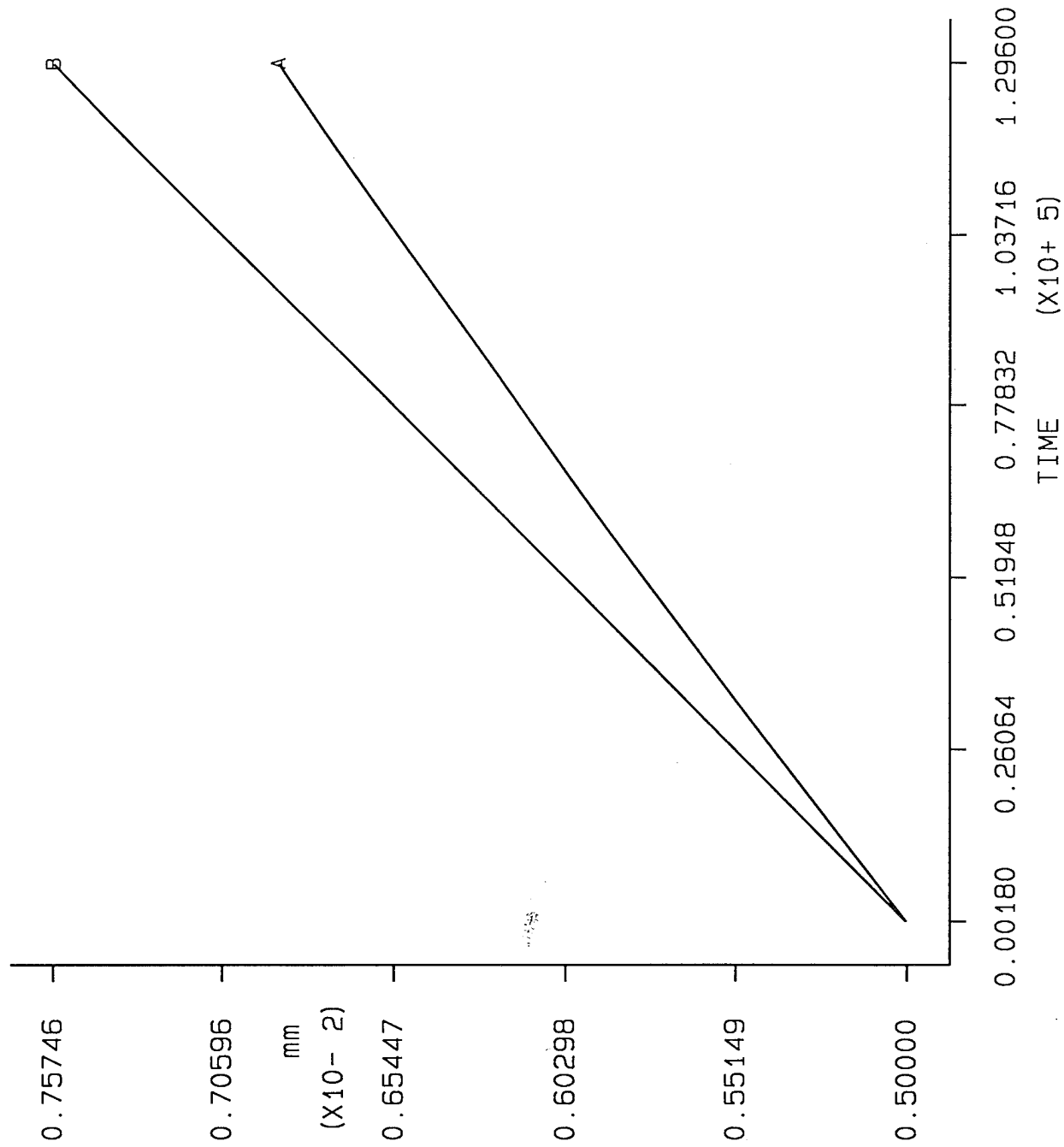
Figure 16 represents the time history of the innermost and outermost radius for a 36 hours time and its referred to the 900°C and 5 torr conditions. It can be observed that the rate of growth of the outermost radius is linear, while the slope of the curve is progressively reduced for the innermost, the rate of reaction being reduced by the decreased diffusion of the reactant.

Figure 21 is a line plot of the fiber radius in the radial direction after 36 hours for the same pressure and temperature shown on Figure 16. The wiggles that appear in the last two nodes are caused by the zero boundary condition imposed on the neighbor nodes of the outer surface, where the equation of the pore radius is not solved. A smarter implementation (completely canceling out the extraneous equations) has not been possible in Phase I study.

It has also to be remarked that the model prevision gives a steep gradient of the fiber radius in the proximity of the outer surface (also accentuated by the numerical overshooting). The reason for this steep gradient can be explained looking at line plot of the reactant concentration, Figure 22, for the same line in the radial direction shown in Figure 21. The outermost fibers always see a reactant concentration which is close to the maximum value and the reactant concentration quickly drops inside the preform, where a different model for diffusion is adopted, giving raise to very different reaction rates.

Figures 15 to 20 show the results of the parametric studies that investigate the effect of the pressure and temperature variations on the rate of densification. The results refer to pressure of 5 and 15 torr and temperature of 880°C , 900°C and 920°C. Some of the significant results are also summarized in the tables.

Fig.15 Total Fiber Radius at T = 880 C P = 5 torr



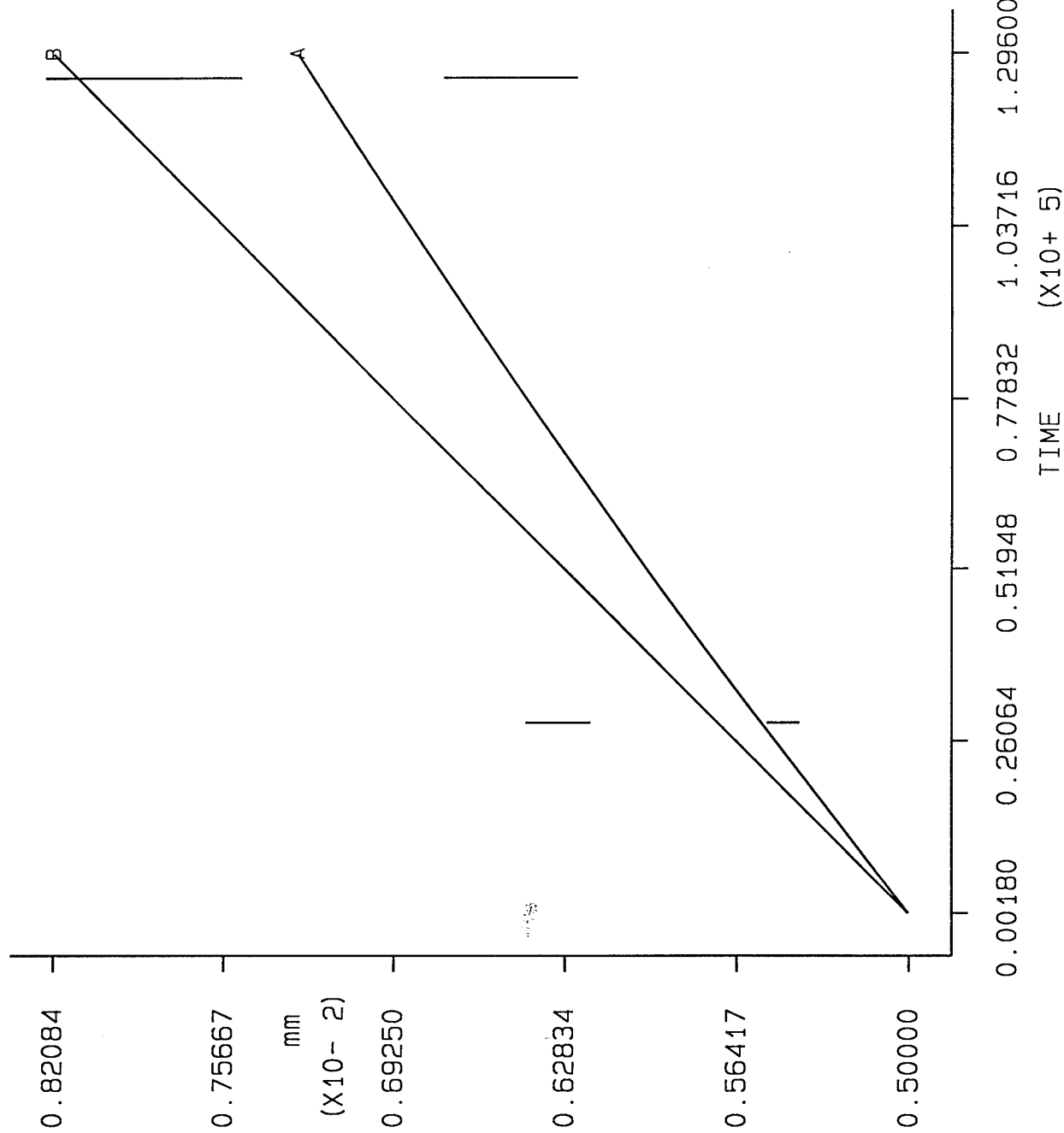
TIME
HISTORY PLOT

FIBER RADIUS

A INNER
B OUTER

FIDAP 7.52
3 Aug 95
17:06:35

Fig.16 Total Fiber Radius at T = 900 C P = 5 torr



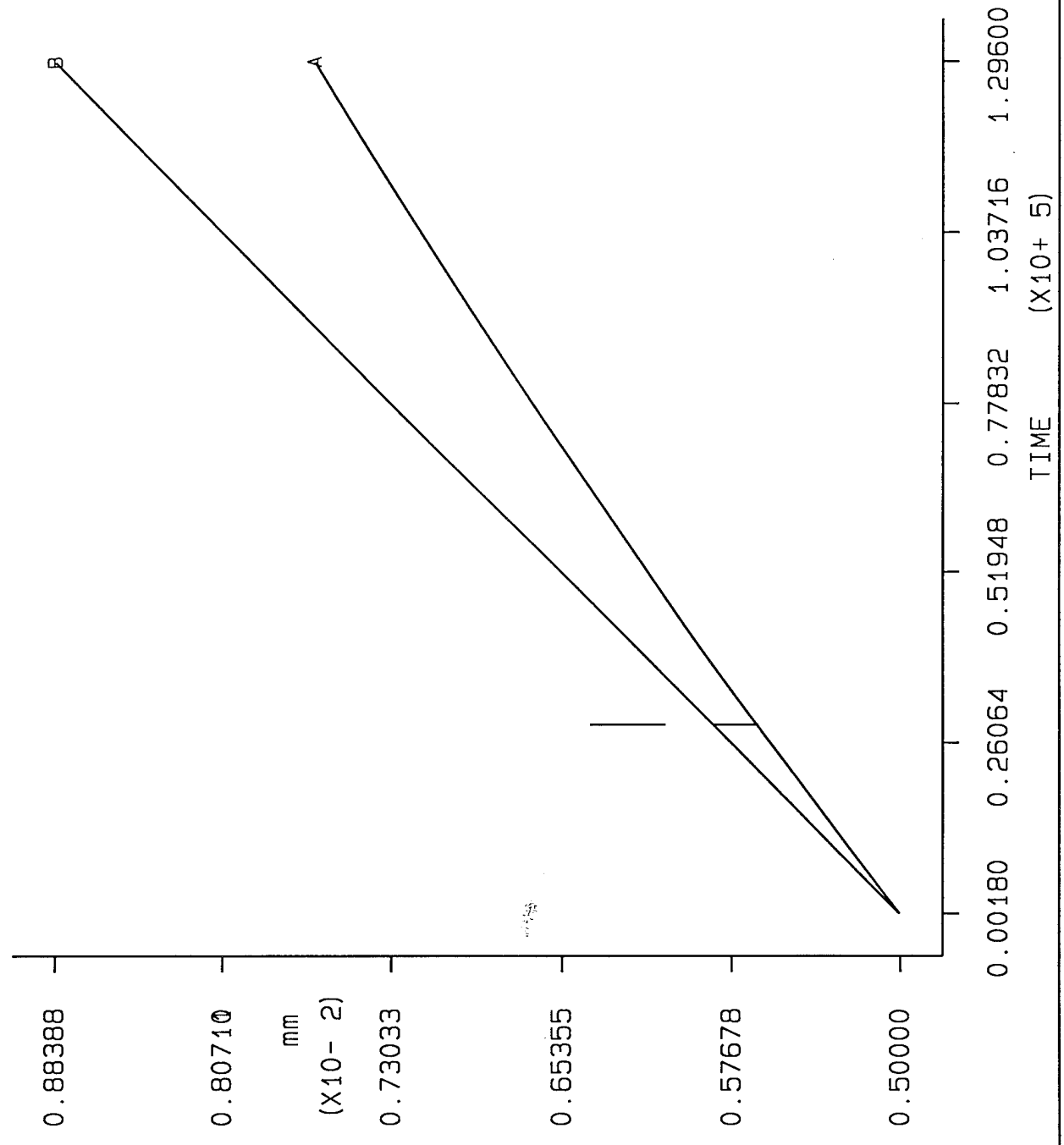
TIME
HISTORY PLOT

FIBER RADIUS

A INNER
B OUTER

FIDAP 7.52
3 Aug 95
17:07:09

Fig.17 Total Fiber Radius at T = 920 C P = 5 torr



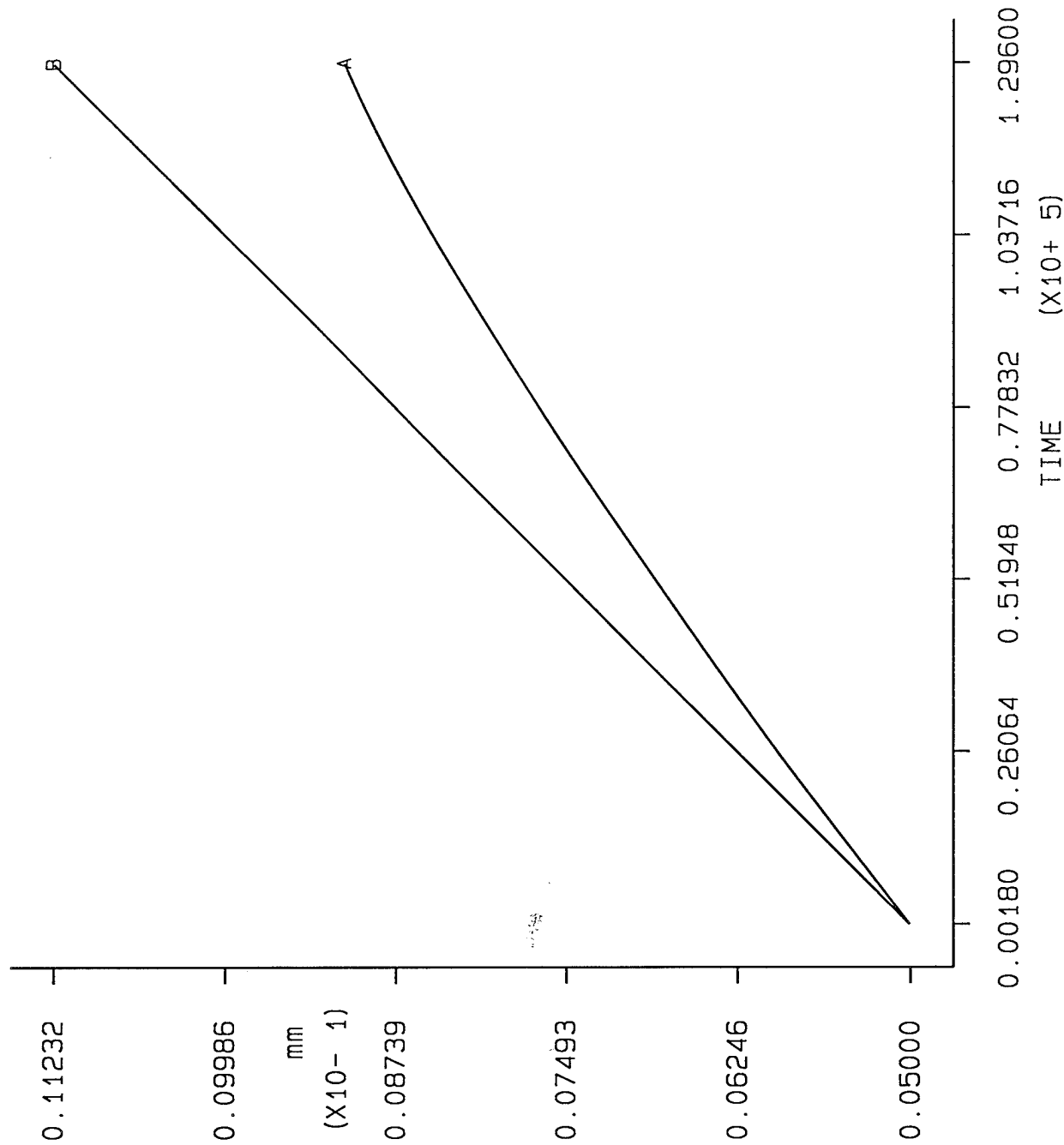
TIME HISTORY PLOT

FIBER RADIUS

A INNER
B OUTER

FIDAP 7.52
3 Aug 95
17:07:42

Fig.18 Total Fiber Radius at T = 880 C P = 15torr



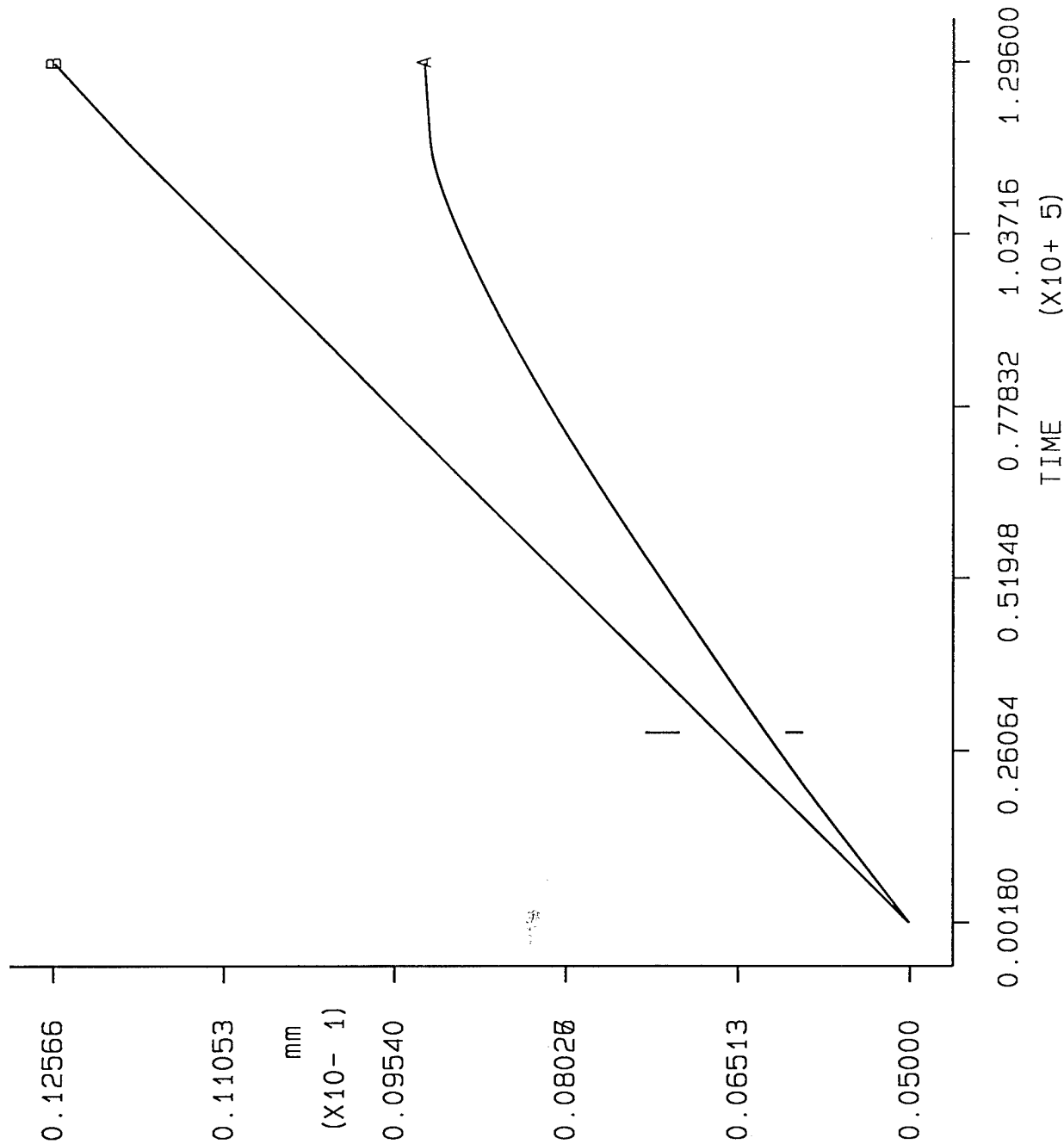
TIME
HISTORY PLOT

FIBER RADIUS

A INNER
B OUTER

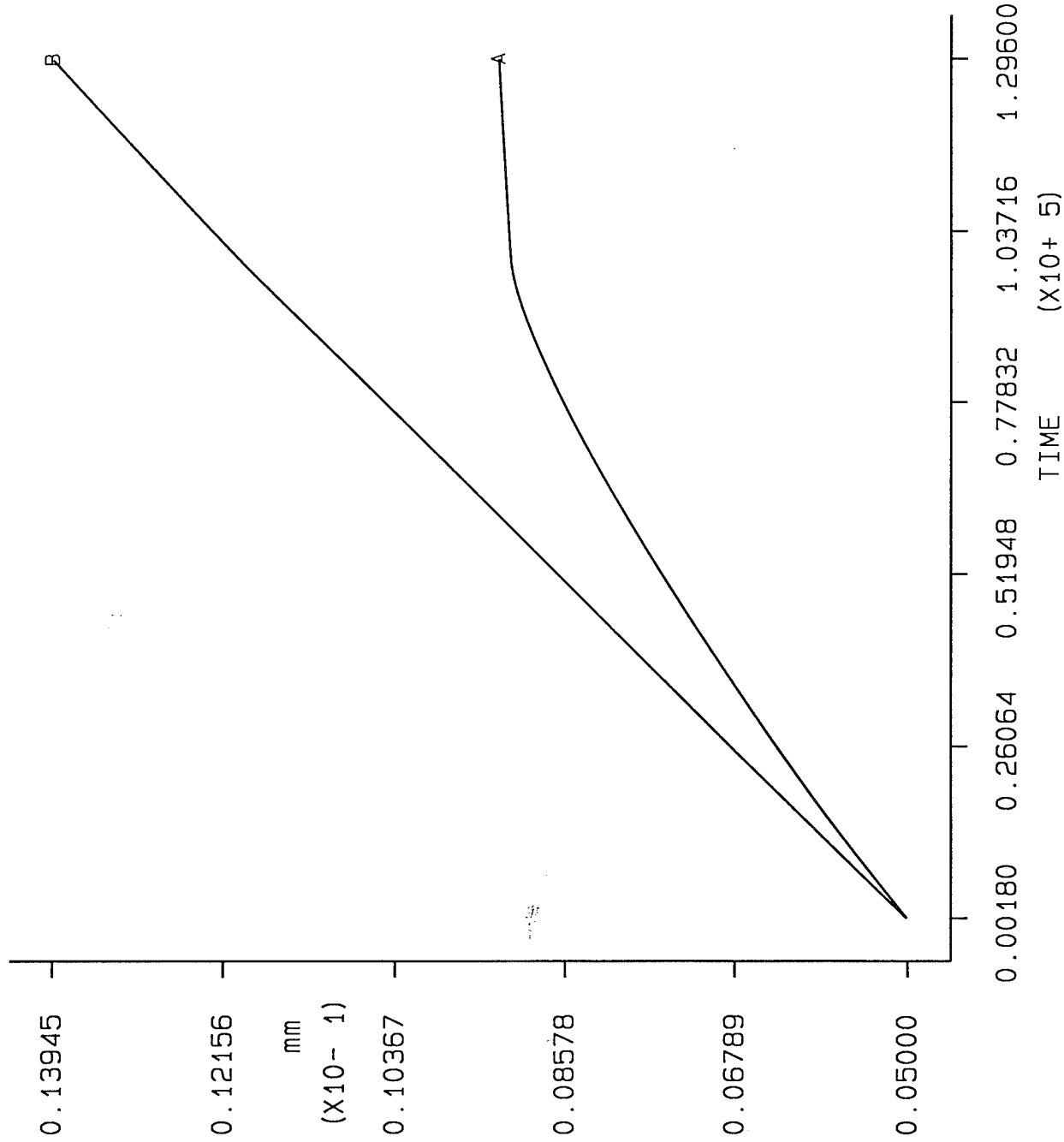
FIDAP 7.52
3 Aug 95
17:08:16

Fig.19 Total Fiber Radius at T = 900 C P = 15torr



FIDAP 7.52
3 Aug 95
17:08:50

Fig.20 Total Fiber Radius at T = 920 C P = 15torr



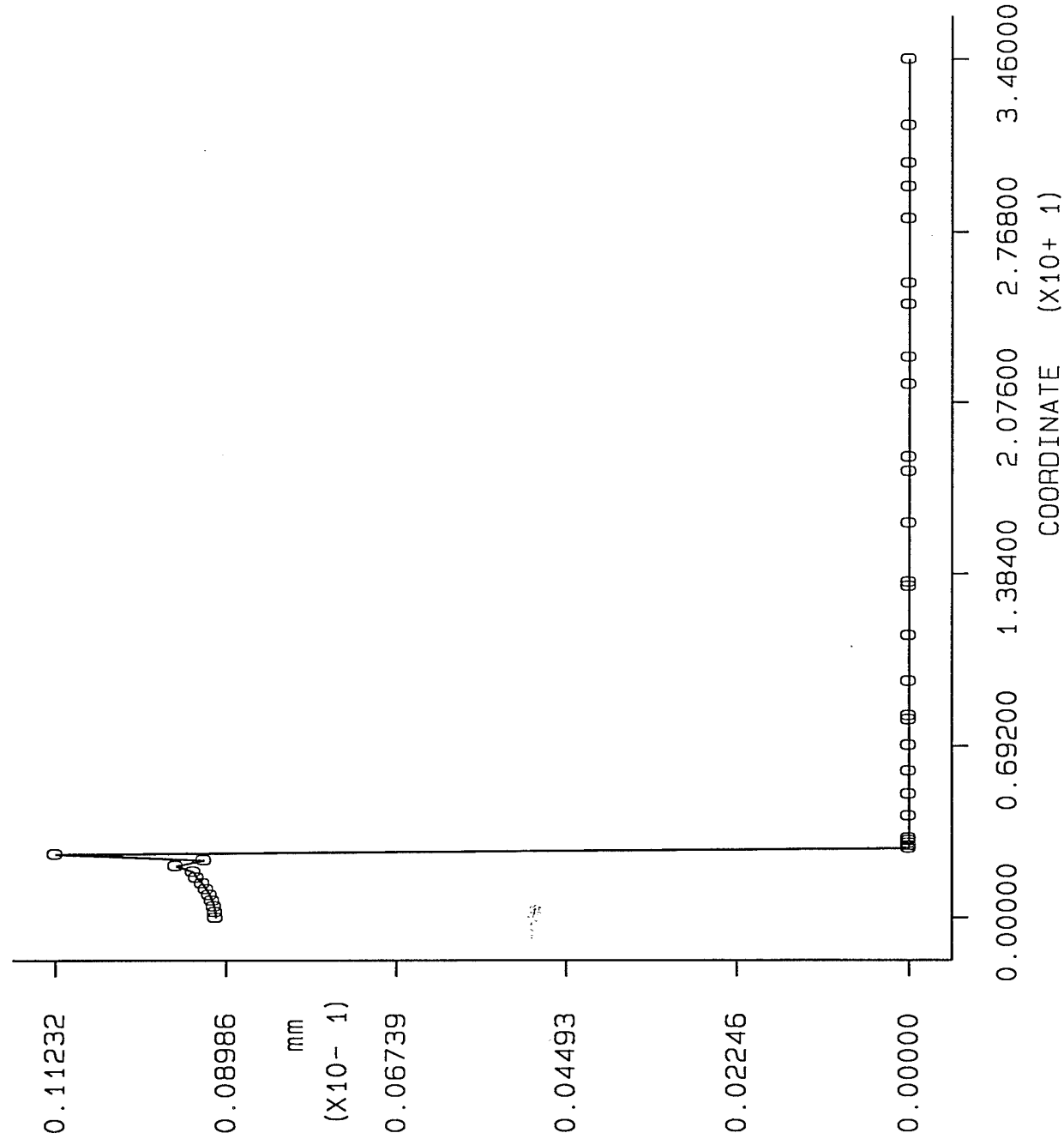
TIME
HISTORY PLOT

FIBER RADIUS

A INNER
B OUTER

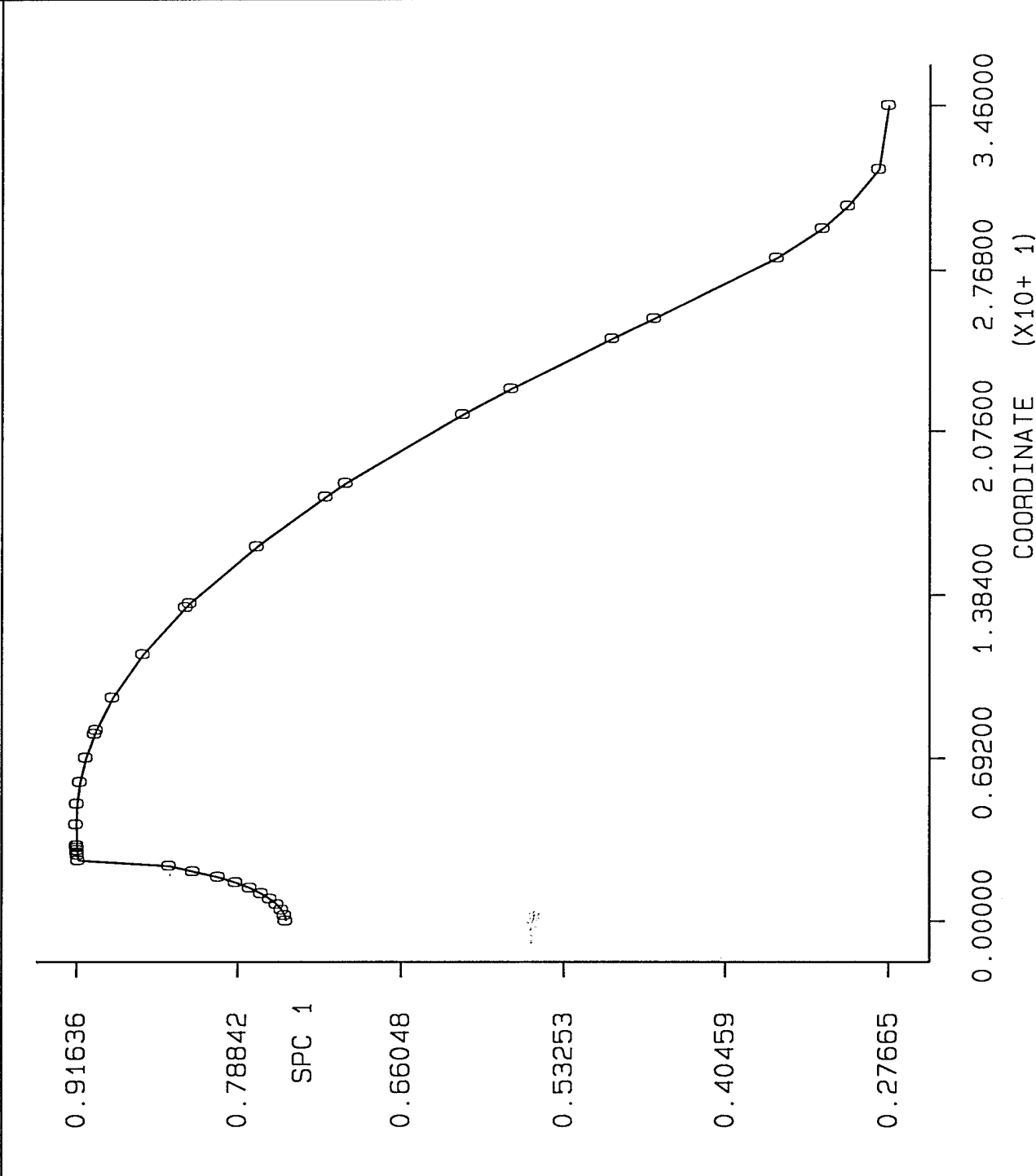
FIDAP 7.52
3 Aug 95
17:09:23

Fig.21 Fiber Radius vs. Radial Coord. T=900 P=15 t=35h



COORDINATE VS. VARIABLE PLOT
FIBER RADIUS
LINE DEFINITION
POINT
X0 0.723E+02
Y0 0.200E+01
DIRECTION
X 0.0000
Y 1.0000
TIME 0.130E+06
FIDAP 7.52
25 Jul 95
11:13:45

Fig.22 React. Conc. vs. Rad. Coord. T=900 P=15 t=35h



COORDINATE VS. VARIABLE PLOT	SPECIES 1
	LINE DEFINITION
	POINT X0 0.723E+02 Y0 0.200E+01
	DIRECTION X 0.0000 Y 1.0000
	TIME 0.130E+06
	FIDAP 7.52 25 Jul 95 11:15:00

In looking at the extended time results for high pressure (15 torr) it must be kept in mind that no "artificial clipping" has been imposed on the maximum value of the fiber radius. While for the inner fibers the reduction in diffusion and the depletion of the reactant provide a mechanism that slows the rate of reaction (see for example the plateaus seen in Figures 19 and 20) shows that the outer fibers linearly grow to the value that seals the external pores. The infiltration process must be considered stopped when this maximum value is reached.

Table 4 Pressure 5 torr Run time 8 hours

Temperature (°C)	Fiber growth inner radius (μm)	Fiber growth outer radius (μm)
880	0.4	0.6
900	0.5	0.7
920	0.6	0.8

Table 5 Pressure 5 torr Run time 35 hour

Temperature (°C)	Fiber growth inner radius (μm)	Fiber growth outer radius (μm)
880	1.8	2.5
900	2.2	3.1
920	2.5	3.7

Table 6 Pressure 15 torr Run time 8 hour

Temperature (°C)	Fiber growth inner radius (μm)	Fiber growth outer radius (μm)
880	1.0	1.4
900	1.2	1.7
920	1.5	2.0

Effect of Temperature

An increase in the reaction temperature decreases the mixture density which appears in Equation 13 for the rate of reaction. This effect is counterbalanced by the much stronger dependence on temperature of the Arrhenius type reaction. The global effect of a 20°C increase in the temperature reaction can be seen as a 20% increase of the rate of deposition.

Effect of Pressure

In the context of this model, the only effect of increasing pressure is a corresponding increase of the mixture density and consequently of the rate of reaction. After 8 hours, it can be seen from Tables 4 to 6 that changing the pressure from 5 to 15 torr translates into a 2.5 increase in the rate of growth of the fiber radius. As already remarked in the comments in the experimental results section [2], a maximum in the rate of deposition as a function of pressure exists at different pressures depending upon temperature and reactant concentration. It is suggested that this effect can be explained invoking a two step reaction and the effect of the residence time of MTS in the reactor. The use of more complex reaction mechanisms has not been investigated during the Phase I study and their implementation into the commercial software code, FIDAP, while being straightforward, has been proposed for investigation in Phase II

CONCLUSIONS

The comparison between Tables 1 to 3 and 4 to 6 reveals an encouraging agreement between the model prediction and the experimental data. The current predictions are restricted to the innermost and outermost fiber radii due to the inability of the current model to adequately represent the voids between the tows. In Figures 15 to 19, the increase in fiber radius resulting from the experimental observation, with its standard deviation, is superimposed on the results of the computations. It appears the model is capable to predict the correct trends of the densification rate as a function of temperature and pressure, while the model slightly overestimates the densification rate as a function of time.

The results appears quite promising in view of the fact that the input parameters have been largely obtained from the literature, with no empirical relationship except the ones regarding the structure of the preform.

It is however our belief that the good agreement between simulation and experimental results obtained from these runs cannot be generalized to other situations without further work. Specifically, the following points seem worthy of further investigation :

- Better reaction data is needed from the literature to include effects not taken into account in the present model, like the "etching" due to the by-products of the reaction, and the presence of a maximum of deposition rate as a function of pressure.
- The adequate representation of the preform geometry is a crucial point which has not received enough attention in most of the models that are based upon the hypothesis of an homogeneous preform. A more detailed description of the porous media, together with measurements of diffusion, permeability and species concentration would be extremely important, also for the simulation of infiltration processes which are not diffusion dominated.

It has finally to be remarked that once the model has been developed and validated, the modifications to the input of the commercial software code, FIDAP, which are needed to simulate a different CVI process can be performed by the user through simple changes to the input file for the software. For example, the simulation of infiltration under pulsed power conditions requires only modification in the boundary conditions for temperature, that can be performed by the analyst on a geometry base, without any need for modifications in the code.

FDI has shown, through comparison with experimental CVI results performed by BIRL, that modifications to an existing commercial fluid dynamics software code, FIDAP, can provide industrial users with a tool to aid in the design and optimization of reactors and CVI processes. Development, testing and refinement of different CVI models within a general purpose CFD code can have a significant impact on the understanding of the process and the optimization of the reactor. If continuation of this work in a Phase II study is initiated, the final results will not be confined to a written report, but will be available for further testing and use on a commercial code, with the possibility, from a user point of view, of having access to the continuously updated, state of the art models for chemical vapor infiltration.

REFERENCES

- [1] Besmann, T.M, Starr, T.L, Matson, L.E., Sheldon, B.W., Processing Science for Chemical Vapor Infiltration, Annual Review, November, 1989, 1990, 1991 and 1992
- [2] Besmann, T.M, Sheldon, B.W., Moss, T.S, Kaster M.D., "Depletion Effects of Silicon Carbide Deposition from Methyltrichlorosilane", J. Am. Ceram. Soc. Vol 75 (10) 1992 (2899-2903)
- [3] Brennfleck, K, Fitzer, E, Schoch G, Dietrich, M in Proc. Int. Conf. on CVD Vol 84-6, (649-656)
- [4] Engelman M.S., FIDAP Theory Manual V. 7.0 Fluid Dynamics International, Evanston IL (1993)
- [5] Melkote R.R, Jensen K.F, in Chemical Vapor Deposition of Refractory Metals and Ceramics" edited by Besmannn, T.M. and Gallois, B.M., (Mater Res.Soc. Symp. Proc. 168) 1990 (67-72)
- [6] Middleman, S., "Interaction of Chemical Kinetics and Diffusion in the Dynamics of Chemical Vapor Infiltration", J. Mater Res., Vol.4, No. 6. 1989 (1515-1524)
- [7] Middleman, S.,Herble, B. and Cheng, H., "Improved Uniformity of Densification of Ceramic Composites Through Control of Initial Preform Porosity Distribution", J. Mater Res., Vol. 5 No 7 1990 (1544-1548)
- [8] Morrel, J, Economou, D, Amundson, N, "A Mathematical model for Chemical Vapor Infiltration with Volume Heating", J Electrochem. Soc. Vol. 139, No 1 1992 (328-337)
- [9] Morrel, J, Economou, D, Amundson, N, "Pulsed power volume-heating chemical vapour Infiltration", J. Mater Res., Vol.7, No. 9 1992 (1515-1524)
- [10] Morrel, J, Economou, D, Amundson, N, "Chemical vapour infiltration with microwave heating", J. Mater Res., Vol.8, No. 5 1993 (1057-1067)

- [11] Sheldon, B.W., "The control of gas phase kinetics to maximize densification during chemical vapor infiltration", J. Mater Res., Vol.5, No.11 1990 (2729-2736)
- [12] Stinton, D.P., Caputo A.J., Lowden, R.A., "Synthesis of Fiber-Reinforced SiC composites by Chemical Vapor Infiltration," Am. Ceram. Bull. Vol. 65 No 2 1986 (347-50)
- [13] Sotirchos S.V., Tomadakis M.M., in Chemical Vapor Deposition of Refractory Metals and Ceramics" edited by Besmann, T.M. and Gallois, B.M., (Mater Res.Soc. Symp. Proc. 168) 1990 (73-78)

LIST OF FIGURES

- Figure 1 Computational Mesh of Reactor
- Figure 2 Centerline Reactor Temperature at Set 1 Conditions
- Figure 3 Centerline Reactor Temperature at Set 2 Conditions
- Figure 4 Velocity Field in Reactor at Set 1 Conditions
- Figure 5 Temperature Contours in Reactor at Set 1 Conditions
- Figure 6 Radial Temperature Profile at Reactor Mid-Height
- Figure 7 Computational Mesh With Preform
- Figure 8 Enlarged View of Computational Mesh Showing Preform Detail
- Figure 9 Optical Micrograph of the 3D-Braided NicalonTM Preform in cross section (magnification 7x)
- Figure 10 Schematic Diagram of CVI Reactor
- Figure 11 Areas of Characterization Within Preform
- Figure 12 Optical Micrograph of II Fibers in Cross Section at a) 900C, b) 920C
- Figure 13 Optical Micrograph of MM Fibers in Cross Section at a) 4-6 torr, b) 15-17 torr
- Figure 14 Optical Micrograph of OO Fibers in Cross-Section at a) 8 hr, b) 35 hr.
- Figure 14A SEM Micrograph of the Preform after 35 Hours
- Figure 15 Total Fiber Radius at T = 880C, P=5 torr
- Figure 16 Total Fiber Radius at T = 900C, P=5 torr
- Figure 17 Total Fiber Radius at T = 920C, P=5 torr

Figure 18 Total Fiber Radius at $T = 880\text{C}$, $P=15$ torr

Figure 19 Total Fiber Radius at $T = 900\text{C}$, $P=15$ torr

Figure 20 Total Fiber Radius at $T = 920\text{C}$, $P=15$ torr

Figure 21 Fiber Radius vs Radial Coordinate $T=920\text{C}$, $P=15$ torr, $t=35$ hr

Figure 22 Reactant Concentration vs Radial Coordinate $T=920\text{C}$,
 $P=15$ torr, $t=35$ hr

LIST OF SYMBOLS

c	Mass Concentration
C	Volume Concentration
E	Activation Energy
f	Body Force
H	Heat Generation Term
k	Reaction Constant
	Thermal Conductivity
m	Sum of Stoichiometric Coefficients in Reaction
M	Molecular Weight
p	Pressure
q	Generic Source Term in Species Equation
r	Fiber Radius
R	Reaction rate
	Gas Constant
S_A	Surface Area per Unit Volume
t	time
T	Temperature
u	Velocity Component
x,y,z	Spatial Coordinates

Greek letters

α	Species Diffusivity
β_T	Volume Expansion Coefficient
δ_{ij}	Kronecker tensor

μ	Viscosity
v	Stoichiometric Coefficient
ρ	Mixture Density
σ_{ij}	Stress Tensor
ϕ	Porosity
Φ	Thiele Modulus

Suffix

i	Component Index
l	Reaction Index
n	Species Index
s	Surface Area
	Solid Properties
0	Reference Conditions
$,$	Derivative Symbol